Geoscience Frontiers 14 (2023) 101479

Contents lists available at ScienceDirect

Geoscience Frontiers

journal homepage: www.elsevier.com/locate/gsf

Research Paper

Correlations among large igneous provinces related to the West Gondwana breakup: A geochemical database reappraisal of Early Cretaceous plumbing systems

Antomat A. Macêdo Filho [a,b,*], Maria Helena B.M. Hollanda [a], Stephen Fraser [b], Alisson L. Oliveira [a], Alanny C.C. Melo [b,c], Alana R. Dantas [a]

[a] Instituto de Geociências, Universidade de São Paulo, 05508-080, São Paulo, Brazil
[b] W.H. Bryan Mining & Geology Research Centre, Sustainable Minerals Institute, The University of Queensland, St Lucia Campus, QLD 4072, Australia
[c] Programa de Pós-Graduação em Geodinâmica e Geofísica, Universidade Federal do Rio Grande do Norte, Campus Universitário S/N, Lagoa Nova, 59078-970 Natal, RN, Brazil

ARTICLE INFO

Article history:
Received 3 February 2022
Revised 4 August 2022
Accepted 12 September 2022
Available online 17 September 2022
Handling Editor: R.D. Nance

Keywords:
LIP-related plumbing systems
Continental tholeiites
Paraná-Etendeka
EQUAMP
Self-organizing maps

ABSTRACT

The opening and spreading of the Atlantic Ocean between Africa and South America evolved during the Early Cretaceous and were preceded by dramatic tholeiitic (mafic) magmatism and minor silicic and alkaline volcanism. These features are presently recognized from the equatorial regions of Brazil and Africa to the Falklands and South Africa. In southeastern South America, continental flood basalts and related plumbing systems constitute the Paraná Magmatic Province (PMP), whose African counterpart is the Etendeka Magmatic Province (EMP). In northeastern Brazil, dike swarms and sill complexes compose the Equatorial Atlantic Magmatic Province (EQUAMP). As a common feature, these provinces are chemically represented by two prevalent magma types: (1) tholeiitic basalts and basaltic andesites with low Ti (TiO_2 < ~2 wt.%), also including transitional Ti tholeiites with TiO_2 ~ 2.7–1.7 wt.%, and low incompatible element contents. This type is predominantly found in the southern PMP and EMP, with minor occurrences in the EQUAMP. (2) Tholeiitic basalts and basaltic andesites with high Ti (TiO_2 > ~2 wt.%) and incompatible element contents. High Ti tholeiites are relevant in the northern PMP and EMP, and dominant in EQUAMP. Evolved rocks (SiO_2 = 57–65 wt.%) interpreted as byproducts of assimilation and/or fractional crystallization (AFC) processes from high Ti tholeiitic magmas, are scarce (but present) in all three provinces. An accurate analysis of multivariable databases collected from the literature for dikes and sills, including major and trace element and radiogenic isotope data, reveals close similarities in their geochemical signatures. In a paleogeographic reconstruction of West Gondwana, the intrusive remnants of the PMP, EMP and EQUAMP are spread over an area of nearly 10×10^6 km^2, forming perhaps the most extensive set of plumbing systems on Earth, with a relatively consistent chronology based on a vast collection of K–Ar and $^{40}Ar/^{39}Ar$ data available in the literature. This work provides the first comprehensive data comparison to support the existence of what may have been a single intercontinental-scale magmatic province of West Gondwana.

1. Introduction

Continental breakup and the initiation of a new ocean are almost always associated with the voluminous magmatism that characterizes Large Igneous Provinces (LIPs). First defined by Coffin and Eldholm (1994), LIPs are massive emplacements of mafic magmas occurring in intraplate settings, manifested as continental flood basalts (CFBs), oceanic basalt outpourings or plateaus, volcanic passive margins, submarine ridges or seamounts. Expanding Coffin and Eldholm's concept, Bryan and Ernst (2008) included extrusive and intrusive silicic (SiO_2 > 65 wt.%) igneous activities not linked to "*...normal seafloor spreading or subduction and massive Precambrian magmatic events...*", in addition to giant dike swarms, sill complexes and layered intrusions, as well as Archean tholeiitic-komatiite volcanism and other intrusive forms such as LIP components (Ernst, 2014). Currently, LIPs are described as 'anomalous' igneous activity covering areas of over 0.1×10^6 km^2 with a total volume (if estimated) of $\geq 1 \times 10^6$ km^3, composed

* Corresponding author at: Instituto de Geociências, Universidade de São Paulo, 05508-080, São Paulo, Brazil.
E-mail address: antomat@alumni.usp.br (A.A. Macêdo Filho).

https://doi.org/10.1016/j.gsf.2022.101479

predominantly, but not exclusively, of mafic (volcanic and/or plutonic) rocks formed in intraplate settings. The anomalous character is also extended to the timing in which a LIP is formed, which is usually reported along a single or multiple pulses of short-lived duration (<5 Myr; often <2 Myr; Bryan and Ferrari, 2013; Ernst et al., 2021).

During the Early Cretaceous, the West Gondwana supercontinent underwent widespread extensional tectonics that led to the modern configuration of the South American and African plates (Seton et al., 2012; Matthews et al., 2016; Müller et al., 2019). The early stage of extensional tectonics, which started before 134 Ma, was also accompanied by the formation of the Paraná Magmatic Province (PMP) and Etendeka Magmatic Province (EMP) (Rocha et al., 2020; Gomes and Vasconcelos, 2021 and references therein). Before the West Gondwana dispersal, these provinces composed a contiguous LIP with bimodal volcanic rocks and related plumbing systems in SE South America and central-southern Africa (Peate et al., 1992; Krob et al., 2020).

Geochemical-focused studies concerning the PMP and EMP were published between the 1980s and 2000s, focusing mainly on CFBs (e.g., Bellieni et al., 1984, 1986; Mantovani et al., 1985, 1988; Petrini et al., 1987; Piccirillo et al., 1988; Hawkesworth et al., 1988; Mantovani and Hawkesworth, 1990; Peate et al., 1992, 1999; Peate and Hawkesworth, 1996; Peate, 1997; Ewart et al., 1998, 2004a,b; Marques et al., 1999; Marsh et al., 2001). In the past 20 years, the geochemical database of the PMP and EMP has notably increased with the addition of data not only on extrusive magmatism (e.g., Marsh et al., 2001; Ewart et al., 2004a,b; Rocha-Júnior et al., 2012, 2013, 2020; De Min et al., 2018) but also on dike swarms and sill complexes (e.g., Thompson et al., 2001; Trumbull et al., 2004, 2007; Guedes et al., 2005, 2016; Santos, 2006; Rosset et al., 2007; Corval et al., 2008; Valente et al., 2009; Backeberg et al., 2011; Keiding et al., 2011, 2013; Velázquez et al., 2011; Muzio et al., 2012, 2017; Almeida et al., 2013a, b,2021; Chaves, 2013, 2014; Marques et al., 2016, 2018; Will et al., 2016; Florisbal et al., 2018; Marsh and Swart, 2018; McMaster et al., 2019; Santiago et al., 2020; Owen-Smith et al., 2021).

Near the equatorial Atlantic margin, Early Cretaceous extensional tectonics led to the development of the NE Brazilian rift system, Benue Trough/Nigeria (Matos, 1992, 2000; Wilson and Guiraud, 1992; Melo et al., 2016), and the emplacement of mafic dike swarms and sill complexes grouped in the Equatorial Atlantic Magmatic Province (EQUAMP; Hollanda et al., 2019). The main elements of the EQUAMP, namely, the Rio Ceará-Mirim dikes and Sardinha sills, have been studied since the 1990s (Bellieni et al., 1990, 1992; Fodor et al., 1990), but only since the 2000s has there been an increase in geochemistry-focused publications (Ernesto et al., 2003; Hollanda et al., 2006; Ngonge et al., 2016; de Castro et al., 2018; Heilbron et al., 2018; Oliveira et al., 2018; Macêdo Filho et al., 2019; Macêdo Filho, 2021; Macêdo Filho and Hollanda, 2022). The EQUAMP plumbing systems may still share geographical space with the Central Atlantic LIP (~201 Ma); however, Early Cretaceous tholeiites present geochemical-isotopic signatures contrasting (e.g., higher contents of incompatible elements and less radiogenic Nd) with those observed in the Jurassic–Triassic components (Macêdo Filho, 2021; Macêdo Filho and Hollanda, 2022).

The evaluation of geochemical databases, geochronological data, and the determination of areal extent (geological mapping) are among the crucial parameters for LIP characterization (Ernst et al., 2005). However, analyzing massive amounts of data by classic methodologies can be laborious depending on the complexity of the database examined. This limitation can be overcome by using machine learning-based tools such as self-organizing maps (SOMs; Kohonen, 1982). An SOM is a nontraditional unsupervised data analysis tool that treats each input sample as a vector in a data space defined by the input variables and then uses measures of vector similarity to find patterns and relationships between the vectors. This computational technique allows an integrated analysis of any multivariate spatial dataset with complex inputs; the method also improves the understanding of the subtle and intricate relationships between disparate datasets (Penn, 2005; Hodgkinson et al., 2013; Kohonen, 2013). SOMs have been extensively applied as analytical (and visualization) tools for high-dimensional data and in exploratory data mining applications such as those identifying correlation patterns and performing clustering analysis to determine anomalies or trends (e.g., Löhr et al., 2010; Friedel, 2011; Carneiro et al., 2012; Melo et al., 2021; Owen-Smith et al., 2021).

In areas strongly affected by erosion, volcanic components may have been lost. Thus, intrusive forms are the best means of retrieving geological information about such LIPs (Ernst, 2014). Plumbing systems, rather than lava flows, may offer high levels of magmatic diversity and less evolved or altered rocks and provide direct information about magma ascent and emplacement (Owen-Smith et al., 2021). Hence, a proper assessment of magma diversity and the areal extent in LIPs should concentrate on (and include) intrusive components. In this study, we applied Ti-based (petrological) classification in conjunction with the SOM approach to organize the PMP, EMP, and EQUAMP geochemical datasets of dike swarms and sill complexes. Making use of major oxides and trace and rare earth elements combined with a qualitative re-evaluation of isotope data (Sr, Nd, and Pb), we investigated the general geological aspects of these provinces to characterize the mafic tholeiitic plumbing systems related to the early opening stage of the South Atlantic Ocean.

2. The Early Cretaceous LIPs related to the West Gondwana breakup

The South Atlantic area presents diverse igneous manifestations, including volcanic and intrusive products of the PMP and EMP, alkaline carbonatites and kimberlites, the Rio Grande Rise-Walvis Ridge, the Tristan archipelago and guyot tracks (Foulger, 2018). In NE Brazil and western/central Africa, mafic igneous manifestations were first named (or genetically correlated) after the nearby Equatorial Atlantic margin (e.g., Maluski et al., 1995; Coulon et al., 1996; Marzoli et al., 2000; Segev, 2002). Recently, Hollanda et al. (2019) reviewed the available information about tholeiitic Early Cretaceous magmatism in NE Brazil combined with an updated LIP classification to propose the EQUAMP. Since the targets considered herein concern intrusive tholeiitic magmatism associated with the PMP, EMP, and EQUAMP, a brief overview of these provinces, their components, and geochemical and geochronological aspects is provided.

2.1. Paraná Magmatic Province

Magmatism in the PMP is mainly fissural with compositionally bimodal components (Peate et al., 1992), as observed on similar rifted continental margins (White and McKenzie, 1989). The PMP remnants are spread across central–southern Brazil, northern Argentina, Uruguay, and eastern Paraguay (Peate, 1997). Flood basalts and sills are mainly reported in the Paraná Basin (Janasi et al., 2007, 2011; Petersohn and Gouvea, 2009; Hartmann et al., 2012, 2013; Rocha-Júnior et al., 2013; Sarmento et al., 2014, 2017; Machado et al., 2015, 2018; Rämö et al., 2016; Baggio et al., 2018; De Min et al., 2018). Recently, Rodrigues et al. (2016) and Rubert et al. (2019) found Cretaceous CFBs and sills in the Parecis Basin (13°S, 54.5°W), expanding the coverage of the PMP toward central South America (Fig. 1). Additionally,

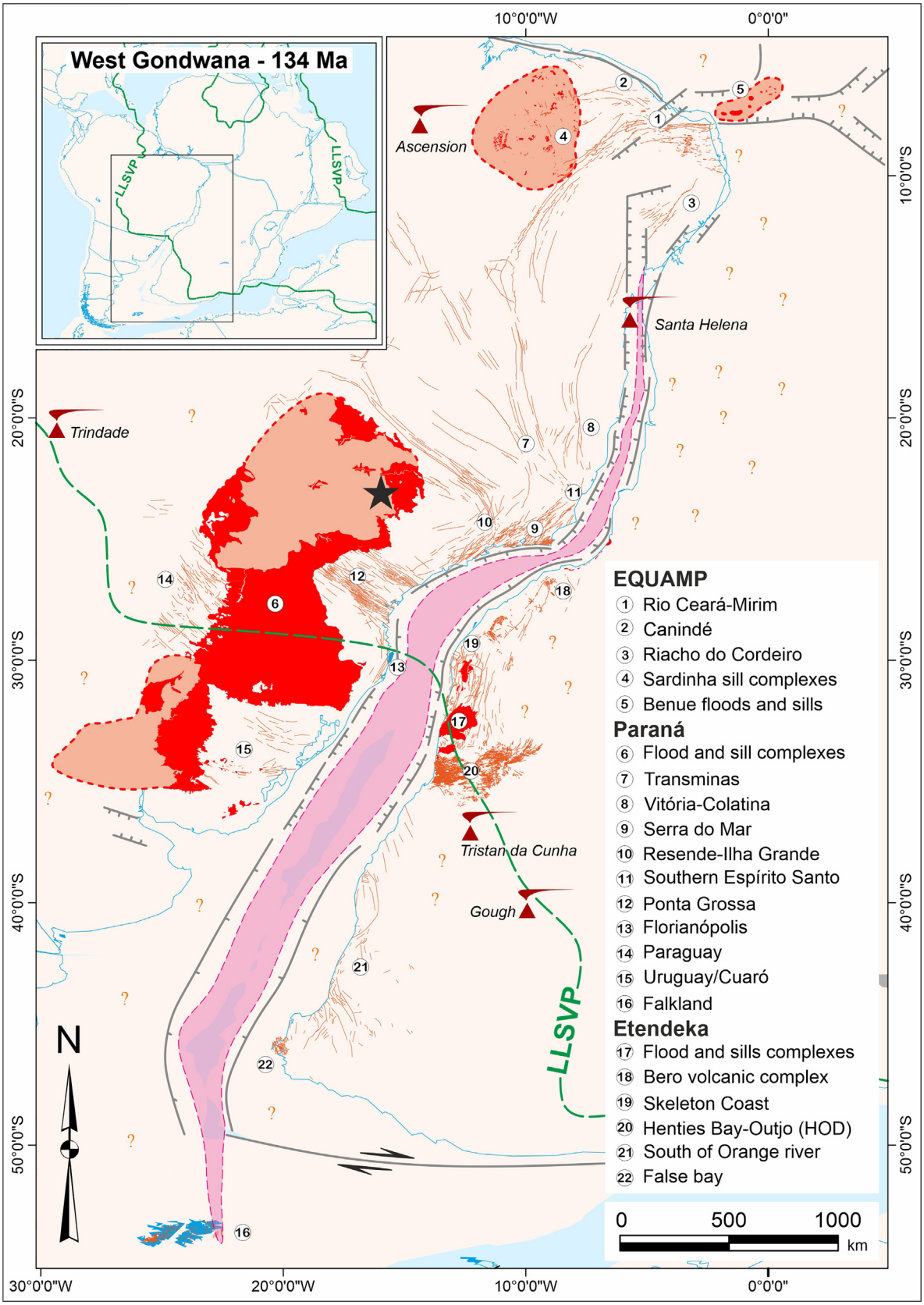

Fig. 1. The West Gondwana reconstruction with a focus on Early Cretaceous tholeiitic magmatism. The red dashed polygons represent regions hosting tholeiitic magmatism that did not crop out, whereas pink dashed polygons represent the offshore magmatic domain. The boundaries of African LLSVPs (Torsvik et al., 2006) are shown by green dashed lines. The reconstruction model at 134 Myr is fully illustrated in the inset (Matthews et al., 2016). The present-day locations of South Atlantic hotspots and major structural features are indicated. The black star in northern Paraná represents the approximate position of the deep upper-mantle low-velocity conduit (VanDecar et al., 1995). (For interpretation of the references to color in this figure legend, the reader is referred to the web version of this article.)

offshore magmatism may occur from 19° to 47° latitude as a volcanic-related rifted margin adjacent to South America (Stica et al., 2014).

Geochronological data of CFBs of the Paraná Basin based on $^{40}Ar/^{39}Ar$ data indicate a peak of activity clustering within a 135–133 Ma interval (see Gomes and Vasconcelos, 2021, for a review). This range overlaps with zircon U–Pb (sensitive high-resolution ion microprobe (SHRIMP)) ages between 135.6 ± 1.8 Ma and 131.3 ± 1.4 Ma obtained for bimodal volcanic rocks (e.g., Pinto et al., 2011; Hartmann et al., 2019) and with high-resolution geochronology (thermal ionization mass spectrometry (TIMS)) ages of 133.65 ± 0.10 Ma and 132.72 ± 0.76 Ma obtained for silicic lavas from the PMP (Janasi et al., 2007; Rocha et al., 2020). However, there has been controversy regarding the ages reported from the U–Pb and $^{40}Ar/^{39}Ar$ methods for the PMP lava pile (Rocha et al., 2020; Gomes and Vasconcelos, 2021).

The geochemical results show variations in the regional composition of the PMP (Bellieni et al., 1984; Bellieni et al., 1986), with low-Ti (LT) tholeiites (TiO_2 < ~2 wt.%) more frequent in the southern portion (plus silicic magmatism; SiO_2 > 64 wt.%), while high-Ti tholeiites (HT) dominate the northern domain (TiO_2 > ~2 wt.%). In Paraná CFBs, Peate (1997) and Peate et al. (1992), Peate et al. (1999) recognized six tholeiitic groups (Ti/Y > 310: Urubici, Pitanga, Paranapanema, and Ribeira; low-Ti/Y < 310: Esmeralda and Gramado) and two silicic volcanic/volcaniclastic suites (low-Ti dacite-rhyolitic Palmas type; HT trachydacitic Chapeco type; TiO_2 threshold of ~1.25 wt.%; Nardy et al., 2011). These magma types were identified by analyzing numerous bivariate plots based on major oxide content (SiO_2, TiO_2, P_2O_5, and $Fe_2O_3^T$), trace elements (Sr, Ba, and Zr) and element ratios (Ti/Zr, Ti/Y, Zr/Y, Sr/Y, and Ba/Y).

The most prominent dike swarms of the PMP are found in Uruguay (Cuaró), Florianópolis, Ponta Grossa, Paraguay, Resende–Ilha Grande, Serra do Mar, Southern Espírito Santo, Transminas, Vitória–Colatina, the Falkland Islands and other less-studied areas (e.g., West Bodoquena and Serra do Caiapó; Ernst and Buchan, 1997). Overall, the tholeiitic plumbing system of the PMP is composed of clinopyroxene, plagioclase, opaque minerals (Fe–Ti oxides and sulfides) and olivine (usually altered) as the main mineral phases, where HT and LT tholeiites form the most common mafic types with subordinate occurrences of silicic–trachyandesitic rocks. Further information about locations, structural trends, and geochemical compositions based on first-order Ti classification and geochronological aspects is provided in Table 1. The spatial distribution of all plumbing systems is illustrated in Fig. 1, which presents an updated map of all igneous manifestations related to the Equatorial/South Atlantic Ocean margin.

2.2. Etendeka Magmatic Province

The EMP comprises CFBs, sills, dikes, silicic volcanism, high-MgO basalt–picrite suites, and alkaline to tholeiitic ring complexes (Ewart et al., 1998, 2004a,b). Offshore breakup volcanism is reported from South Africa to Gabon (Gladczenko et al., 1997; Fernandez et al., 2020). The main dike swarms (Fig. 1) are those at False Bay, south of the Orange River systems (Saldanha Bay, Piketberg–Ceres, Cedarberg, Knersvlakte, Doring–Tanqua, Garies, Mehlberg, and Meob–Conception Bay; Trumbull et al., 2007), Henties Bay-Outjo (HOD), the Skeleton Coast, SW Angola, and several other swarms near the Atlantic margin (Trumbull et al., 2004, 2007; Backeberg et al., 2011; Will et al., 2016; McMaster et al., 2019).

The geochronological results for the EMP show ages from 134 Ma to 132 Ma (Table 1), analogous to those reported for the PMP. Some magmas on the African side also yield slightly older ages of 135 ± 4 Ma and 135.2 ± 0.7 Ma (Reid and Rex, 1994; Will et al., 2016), similar to those observed in LT Gramado basalts from the PMP (see Gomes and Vasconcelos, 2021, for a review). According to Marsh et al. (2001), the EMP may be subdivided into southern (mainly LT basalts) and northern domains (mainly HT basalts) with the E–W boundary at latitude 19°21.6′ S crossing Mowe Bay (Namibia). These authors point out that the EMP has a larger variety of silicic and LT mafic magmatism than that observed in South American examples. The EMP magmatism is composed of 8 mafic groups, including HT (Khumib) tholeiites, LT tholeiites (Tafelberg, Kuidas, Horingbaai, Huab, Taefelkop, Albin and Esmeralda), and high-MgO basalts/picrites (MgO ≥ 13 wt.%), and 17 silicic magmas. The silicic magmas are characterized by parameters such as the major elements SiO_2, TiO_2, and P_2O_5, alkalis, and MgO; large-ion lithophile elements (LILEs) and high field strength element (HFSE) abundances (e.g., Zr, Sr, Rb, and Nb); element ratios (e.g., Zr/Y and Ti/Y); and isotopes (Sr–Nd). These magmas are also identified in sill and dike swarms of the Etendeka area (Table 1); however, the dominant group is associated with LT tholeiites (e.g., Erlank et al., 1984; Kirstein et al., 2001; Ewart et al., 2004a; Trumbull et al., 2004, 2007; Backeberg et al., 2011; Will et al., 2016; McMaster et al., 2019).

2.3. Equatorial Atlantic magmatic Province

The main EQUAMP components include the Rio Ceará-Mirim, Canindé, and Riacho do Cordeiro dike swarms and the Sardinha sills (and dikes) (Fig. 1). Previous geochemical classifications are extensively based on TiO_2 content (threshold at 2 wt.%) (Bellieni et al., 1990, 1992; Fodor et al., 1990; Ernesto et al., 2003; Hollanda et al., 2006, 2019; Ngonge et al., 2016; de Castro et al., 2018; Heilbron et al., 2018; Oliveira et al., 2018; Macêdo Filho et al., 2019; Macêdo Filho and Hollanda, 2022), trace element abundances (plus element ratios; e.g., Ti/Y and Ti/Zr) and isotopes (Sr–Nd–Pb) to distinguish dominant HT (plus minor evolved rocks (ERs)) and LT rocks composed of clinopyroxene, plagioclase, opaque minerals and rare and altered olivine (Macêdo Filho, 2021; Macêdo Filho and Hollanda, 2022). The reported $^{40}Ar/^{39}Ar$ ages of the Rio Ceará-Mirim and Sardinha intrusions range from 134 Ma to 126 Ma (Smith et al., 2001; Souza et al., 2003; Ngonge et al., 2016) and 136–119 Ma (Baksi and Archibald, 1997; Heilbron et al., 2018; Fernandes et al., 2020), respectively (Table 1).

The Rio Ceará-Mirim propagates toward the São Francisco Craton (Hollanda et al., 2019; Melo et al., 2021, 2022; Oliveira et al., 2021; Pessano et al., 2021) as far as the city of Barreiras (12°S, 44.9°W); this trend suggests lateral continuation with the Transminas dikes (Fig. 1), which is also supported by geochemical isotopic data (Macêdo Filho and Hollanda, 2022). The single plumbing system has a total length of at least 2,200 km and hence is the largest dike swarm related to the opening of the South Atlantic Ocean (Macêdo Filho, 2021).

The Riacho do Cordeiro dike swarm is a coast-parallel strike swarm (N45°E) essentially composed of LT tholeiites (TiO_2 < 2-wt.%; Dantas, 2021) with K–Ar ages between 119 Ma and 105 Ma (Mizusaki and Saracchini, 1991; Hollanda et al., 2019) and $^{40}Ar/^{39}Ar$ ages of ~133 Ma (Dantas, 2021), therefore supporting an Early Cretaceous derivation. In its southern termination, the Riacho do Cordeiro dike swarm is covered by the Tucano Basin; however, magnetic anomalies reappear near the town of Araci (11.3°S, 38.9°W) and propagate to the surroundings of Amargosa (13°S, 39.3°W). Notwithstanding, approximately 180 km to the south, several anomalies reappear and mark the appearance of the northernmost Vitória-Colatina dike swarm. In the Vitória-Colatina dike swarm, Belém (2014) reported $^{40}Ar/^{39}Ar$ and U–Pb geochronological data, stating that the younger ($^{40}Ar/^{39}Ar$) Cretaceous dates are concerned with the effect of Ar-reset, while Cambrian U–Pb dates should be considered crystallization ages.

Table 1
Geochemical and geochronological synthesis of Paraná, Etendeka, and Equatorial Atlantic tholeiitic plumbing systems. Geochemical groups are classified according TiO_2 content and degree of fractionation as high–Ti tholeiites (HT; TiO_2 > ~2 wt.%), low–Ti tholeiites (LT; TiO_2 < ~2 wt.%) and evolved rocks (ER; SiO_2 > 56.5–63 wt.%).

Plumbing System	Location	Prevalent geochemical groups	General orientation	Geochronology				
				Age (Ma)	Confidence level	Method	Dated material	Reference
	Paraná							
Falkland	Eastern Falkland Islands	LT[1]	N05–15 W	~135[a]	-	$^{40}Ar/^{39}Ar$	pl	Richards et al. (2013)
				121.3 ± 1.2[b]	–	$^{40}Ar/^{39}Ar$	pl	Stone et al. (2008)
Uruguay (Cuaró)	Central Uruguay	LT[2]	N45–75 W	131.6 ± 1.3[c]	–	$^{40}Ar/^{39}Ar$	–	Ures et al. (1997) apud Masquelin et al. (2009)
Florianópolis	Coastal area of Santa Catarina state (BR)		N15–55E	129.4 ± 0.3[d]	–	$^{40}Ar/^{39}Ar$	pl	Deckart et al. (1998)
				119.0 ± 0.9 to 128.3 ± 0.5[b]	2σ	$^{40}Ar/^{39}Ar$	pl	Raposo et al. (1998)
		HT, LT, ER[3, 4]		134.1 ± 0.9[e]	2σ	U–Pb, TIMS	zr, bd	Florisbal et al. (2014)
Ponta Grossa	Paraná and southern São Paulo states (BR)	HT, LT, ER[5]	N60W	131.4 ± 0.4 to 129.2 ± 0.4[b]	1σ	$^{40}Ar/^{39}Ar$	pl	Renne et al. (1996a)
				133.9 ± 0.2[e] 133.4 ± 0.2[e]	2σ	U–Pb, TIMS	zr, bd	Almeida et al. (2018)
Resende–Ilha Grande	Easten São Paulo state (BR)	HT[6]	N30W to N70–20 W	156.5 ± 7.4 to 144 ± 3.2[d]	1σ	$^{40}Ar/^{39}Ar$	wt	Guedes et al. (2016)
Serra do Mar	Rio de Janeiro state (BR)	HT, LT[7, 8, 9, 10, 11]	N30–50E	132.23 ± 0.6[f] to 132.1 ± 1.5[d]	-	$^{40}Ar/^{39}Ar$	amp	Carvas (2016)
				~134.5 to 129.8[a,e]	1σ	$^{40}Ar/^{39}Ar$	pl	Deckart et al. (1998)
				137.8 ± 0.7 to 127.7 ± 4.6 [g]	1σ	$^{40}Ar/^{39}Ar$	pl, wt	Turner et al. (1994)
				130.2 ± 4.6 [d] 130.3 ± 2.9 [d] 135.9 ± 8.4[f] 128.4 ± 6.5[b] 122.4 ± 9.1[f] 134.5 ± 1.7 [d] 110.0 ± 6.6 [d] 130.3 ± 1.6 [d] 120.4 ± 2.5 [d] 122.1 ± 3.5[b] 116.7 ± 3.1[f] 124.3 ± 0.8[f] 120.6 ± 3.0 [d]	-	$^{40}Ar/^{39}Ar$	pl	Almeida et al. (2021)
Southern Espírito Santo	Espírito Santo state (BR)	LT, HT[12]	N65W	141.9 ± 1.9 [h]	2σ	U–Pb, LA–ICP–MS	zr	Santiago et al. (2020)
Transminas	Minas Gerais state (BR)	HT[13, 14]	N05–60 W	131.92 ± 3.63 [g] 128.43 ± 8.46 [g]	2σ	$^{40}Ar/^{39}Ar$	pl	Coelho and Chaves (2017)
				130.3 ± 0.6[b] 129.8 ± 0.3[b]	1σ	$^{40}Ar/^{39}Ar$	pl	Rosset et al. (2007)
Vitória–Colatina	Espírito Santo and eastern Minas Gerais (BR)	LT[15]	N05–20 W	134.92 ± 0.26[b] 133.5 ± 0.40[d]	1σ	$^{40}Ar/^{39}Ar$	pl, wt	Belém (2014)
	Etendeka							
False Bay	SW coast of South Africa	LT, HT[16, 17]	N40–70 W	131.3 ± 1.3 [g]	1σ	$^{40}Ar/^{39}Ar$	pl	Stewart et al. (1996)
Cedarberg	Africa–SW Namibia	LT[16]	N40–70 W	–	-	-	–	–
Piketberg–Ceres			NS	–	-	-	–	–
Mehlberg			NS and N10W	134 ± 3[d]	-	-	–	Reid and Rex (1994)
Meob–Conception Bay			NS	–	-	-	–	–
Henties Bay–Outjo (HOD)	Namibia	LT, HT, ER[18, 19]	N40–70 W and N30–70E	~125–130[a]	2σ	$^{40}Ar/^{39}Ar$	pl	Erlank et al. (1984)
HOD (Huab sills)	Namibia	LT[18, 19]	–	132.0 ± 0.7[b]	2σ	$^{40}Ar/^{39}Ar$	pl	Renne et al. (1996b)
Etendeka Gabbro	Namibia	LT[20]	–	130.5 ± 0.8[b]	2σ	$^{40}Ar/^{39}Ar$	pl	Kirstein et al. (2001)
Möwe Bay	Namibia–Angola	LT, HT, ER[21]	NS and N10W [a]	135.2 ± 0.7[b] 130.5 ± 0.3[b] 124.1 ± 0.8[b] 113.0 ± 0.5[b]	1σ	$^{40}Ar/^{39}Ar$	wt	Will et al. (2016)
Skeleton Coast	Namibia–Angola	LT, HT, ER[22, 23, 24]	NS and N10W; N25W	129.5 ± 1.5[b]	2σ	$^{40}Ar/^{39}Ar$	pl	Kirstein et al. (2001)
Kwanza basin basalts	Western Angola	HT, LT[25]	NS and N60–80 W	126.1 ± 4[b] 131.9 ± 1.6 [g] 131.1 ± 1.0 [g]	2σ	$^{40}Ar/^{39}Ar$	pl	Marzoli et al. (1999b)
Bero volcanic complex	SW Angola	LT, HT, ER[26]	–	–	-	-	–	–

(*continued on next page*)

Table 1 (*continued*)

Plumbing System	Location	Prevalent geochemical groups	General orientation	Geochronology				
				Age (Ma)	Confidence level	Method	Dated material	Reference
	Equatorial Atlantic							
Rio Ceará–Mirim	Rio Grande do Norte, Ceará, Piauí and Bahia (northern) states. (BR)	HT, LT, ER [27, 28, 29, 30]	E–W	130.9 ± 2.9 [g]	1σ	$^{40}Ar/^{39}Ar$	amp, py	Smith et al. (2001)
				129.8 ± 1.8 [g]				
				132.2 ± 1.0[f]	-	$^{40}Ar/^{39}Ar$	amp	Souza et al. (2003)
				126.9 ± 4[a]	2σ	$^{40}Ar/^{39}Ar$	pl	Ngonge et al. (2016)
			N45E	136	–	K–Ar	wt	Sial (1976)
				134–120	1σ	K–Ar	wt	Oliveira (1992)
Canindé	Northern Ceará state (BR)	HT [30]	N70W	141–126	1σ	K–Ar	wt	Oliveira et al. (2021)
Riacho do Cordeiro	Pernambuco, Alagoas, Sergipe and (NE) Bahia. (BR)	LT[31]	N35E	105.4 ± 9.5	–	K–Ar	wt	Mizusaki and Saracchini (1991)
				119 ± 2	–	K–Ar	wt	Hollanda et al. (2019)
				~133[a]	-	$^{40}Ar/^{39}Ar$	pl	Dantas (2021)
Sardinha sill complexes (eastern Parnaíba Basin)	Piauí and eastern Maranhão (BR)	HT, ER[30, 32, 33, 34, 35, 36, 37]	–	128.4 ± 0.5[f]	1σ	$^{40}Ar/^{39}Ar$	wt	Baksi and Archibald (1997)
				124.6 ± 0.6[b]				
				124.9 ± 0.9[b]				
				159.0 ± 0.6[b]				
				159.6 ± 0.7[b]				
				120.0 ± 0.5[f]				
				119.6 ± 0.8[b]		$^{40}Ar/^{39}Ar$	pl, wt	Heilbron et al. (2018)
				128.0 ± 1.3[d]				
				126.0 ± 2.7[b]				
				128.8 ± 2.3[b]				
				125.7 ± 2.7[d]				
				128.3 ± 0.7[d]				
				128.9 ± 1.3[d]				
				132.95 ± 0.43[b]	2σ	$^{40}Ar/^{39}Ar$	wt	Fernandes et al. (2020)
				132.07 ± 0.43 [g]				
				136.86 ± 0.35 [g]				
				133.79 ± 0.30 [g]				
Benue (bimodal) volcanics	Nigeria	HT, LT[38]	–	106.0 ± 1.5[f]	-	$^{40}Ar/^{39}Ar$	pl, Kf	Maluski et al. (1995)
				123.1 ± 1.6[d]				
				146.7 ± 1.6[b]				
				138.0 ± 1.8[d]				
				130.7 ± 2.7[d]				
				143.1 ± 1.5[b]				
				137.8 ± 1.9[b]				

Geochemical/geological information sources: Paraná: 1 – Stone et al. (2008); 2 – Muzio et al. (2012), Muzio et al. (2017); 3 – Marques et al. (2018); 4 – Florisbal et al. (2018); 5 – Piccirillo et al. (1990); 6 – Guedes et al. (2016); 7 – Santos (2006); 8 – Corval et al. (2008), Corval (2009); 9 – Ngonge et al. (2013); 10 – Carvas (2016); 11 – Almeida et al. (2021); 12 – Santiago et al. (2020); 13 – Rosset et al. (2007); 14 – Marques et al. (2016); 15 – Valente et al. (2009). Etendeka: 16 – Trumbull et al. (2007); 17 – Backeberg et al. (2011); 18 – Trumbull et al. (2004); 19 – Ewart et al. (2004a); 20 – Kirstein et al. (2001); 21 – Ewart et al. (1998); 22 – Will et al. (2016); 23 – Will et al. (2016); 24 – McMaster et al. (2019); 25 – Marzoli et al. (1999b); 26 – Marsh and Swart (2018). Equatorial Atlantic: 27 – Bellieni et al. (1992); 28 – Hollanda et al. (2003); 29 – Ngonge et al. (2016); 30 – Macêdo Filho (2021); 31 – Dantas (2021); 32 – Fodor et al. (1990); 33 – Bellieni et al. (1990); 34 – Ernesto et al. (2003); 35 – Heilbron et al. (2018); 36 – Oliveira et al. (2018); 37 – Macêdo Filho et al. (2019); 38 (Benue) – Coulon et al. (1996). a – Authors recommended age from multiple samples dated; b – Plateau age; c – Argon spectra not shown; d – Weighted mean of not contiguous steps; e – Concordia age of multigrain zircon and baddeleyite fractions; f – Integrated age; g – Isochron age; h – Concordia age of zircon crystals; pl – plagioclase; zr – zircon; bd – baddeleyite; wt – whole–rock; amp – amphibole; py – pyrite; Kf – K–feldspar.

However, the $^{40}Ar/^{39}Ar$ age spectra for these rocks generally produced good plateaus, with minor resets in low- or high-temperature steps. In addition, the dated zircon crystals have rounded shapes that are not expected from a rapid crystallization mafic magma. Moreover, the internal structures observed in cathodoluminescence images show zonation patterns, again not compatible with a rapid cooling magmatic environment. In general, zircons crystallized from mafic subvolcanic magmas tend to be acicular shaped (frequently euhedral to skeletal) with no internal zonation. Hence, we assume that the U–Pb ages are derived from inherited zircons and that the $^{40}Ar/^{39}Ar$ ages are the actual dike emplacement ages for these dikes. These findings suggest that the Riacho do Cordeiro and Vitória-Colatina dikes form a single plumbing system that is at least 1,600 km long and parallel to subparallel to the eastern coastline of South America in the adjacent segment (Macêdo Filho, 2021).

The Benue Trough in Nigeria is the most magmatically active area of the West and Central African rift systems (Wilson and Guiraud, 1992), where Early Cretaceous magmatism has been reported (e.g., Benkhelil et al., 1988; Guiraud and Maurin, 1992; Maluski et al., 1995; Coulon et al., 1996; Loule and Pospisil, 2013). In satellite images, mafic dike swarms can be mapped until the plateau state in central Nigeria. According to Maluski et al. (1995), the Mesozoic bimodal igneous activity of the Benue rift erupted in the Tithonian–Aptian interval with $^{40}Ar/^{39}Ar$ ages between 146.7 ± 1.6 Ma and 123.1 ± 1.6 Ma. Considering the EQUAMP elements in NE Brazil and Nigeria, the total area in which remnants are present exceeds 1×10^6 km^2 in the West Gondwana realm.

3. Materials and methods

3.1. Sample selection and screening

This work was developed based on whole-rock major oxides (SiO_2, Al_2O_3, $Fe_2O_3^T$, MnO, MgO, CaO, Na_2O, K_2O, TiO_2, and P_2O_5), trace elements (V, Cr, Co, Ni, Cu, Pb, Zn, Rb, Sr, Cs, Y, Zr, Nb, Ba, Hf, Ta, Th, and U) and rare earth elements (REEs; La, Ce, Pr, Nd, Sm, Eu, Gd, Tb, Dy, Ho, Er, Tm, Yb, and Lu) from the literature

published mainly from 2004 to 2021 (Almeida et al., 2021; Backeberg et al., 2011; Corval, 2009; Corval et al., 2008; Ewart et al., 2004a; Florisbal et al., 2018; Guedes et al., 2016; Hartmann et al., 2012; Keiding et al., 2011, 2013; Machado et al., 2007; Marques et al., 2018; Marsh and Swart, 2018; McMaster et al., 2019; Muzio et al., 2017; Ngonge et al., 2013; Owen-Smith et al., 2021; Petersohn and Gouvea, 2009; Piccirillo et al., 1990; Renne et al., 1996a; Renner, 2010; Rosset et al., 2007; Santiago et al., 2020; Santos, 2006; Sarmento et al., 2014, 2017, 2020, Thompson et al., 2001, 2007, Trumbull et al., 2004, 2007; Valente et al., 2009; Wigand et al., 2004; Zhou et al., 2020; Carvas, 2016; de Janasi et al., 2007; Stone, 2013). The compiled datasets were obtained via X-ray fluorescence (XRF) for major oxide determination (and some trace elements in a few publications) and other more precise tools, such as inductively coupled plasma (MS), atomic emission spectrometry (AES), optical emission spectrometry (OES), emission spectrometry (ES) and instrumental neutron activation analysis (INAA), for the determination of major oxides, trace elements and REEs.

Highly magnesian samples (MgO > 10.5 wt.%) are not considered in this study because picritic magmas are virtually absent in the EQUAMP and PMP. These filtering criteria also eliminated samples potentially affected by ferromagnesian crystal accumulation. We reject potentially altered rocks by removing samples with loss on ignition (LOI) > 3.5 wt.% and correct all samples to a volatile-free basis. Contemporaneous silicic (SiO_2 > 65.5 wt.%) and alkaline magmas are also removed from the database because they are virtually absent in the EQUAMP and beyond the scope of tholeiitic magmatism. Nevertheless, we consider ERs (SiO_2 = 57–65.5 wt.%) as fractional crystallization products from tholeiitic parental melts that are recognized in the three provinces. Outliers that were not explained in their original publications were removed. Moreover, as the EQUAMP is an exclusively intrusive LIP, we consider only data from dikes and sill complexes of the PMP and EMP (956 samples) to make a proper comparison (Supplementary Data Table A1).

For data compilation for the EQUAMP, we integrate datasets of the EW-Rio Ceará-Mirim (Hollanda et al., 2006; Ngonge et al., 2016), NE-Rio Ceará-Mirim, Canindé (Macêdo Filho and Hollanda, 2022) and Riacho do Cordeiro dike swarms (Dantas, 2021) and Sardinha sill samples (Macêdo Filho et al., 2019; Macêdo Filho, 2021) because they are characterized by the same sampling strategy and analytical protocols. We also integrated other datasets of Sardinha sills available in Heilbron et al. (2018) and Oliveira et al. (2018). The Mesozoic magmatic activity in NE Brazil encompasses an older Jurassic event associated with CFBs and intrusions of Central Atlantic Magmatic Province (Marzoli et al., 1999a) and Early Cretaceous (EQUAMP) sills and dikes. Consequently, a mandatory step in the validation of the EQUAMP database involves recognizing and removing samples potentially belonging to the Central Atlantic LIP, which can promote 'noise' in the EQUAMP dataset (Macêdo Filho, 2021). The database was processed by a thorough revaluation and comparison of the overall geochemical and isotopic compositions to those from previous works published for the CAMP in NE Brazil (Fodor et al., 1990; Bellieni et al., 1992; De Min et al., 2003; Ernesto et al., 2003; Merle et al., 2011; Klein et al., 2013; Heilbron et al., 2018; Oliveira et al., 2018). This age provinciality screening is also supported by recent geochronological approaches used in dike swarms intrusive in Borborema Province (Oliveira et al., 2021). Additionally, we considered six samples of Early Cretaceous mafic volcanic rocks of northern Benue compiled from Coulon et al. (1996) but only observed the geochemical behavior and regional distribution of magma types. Unfortunately, the paucity of geochemical and geological information about Early Cretaceous tholeiites in the Nigeria region precludes drawing accurate correlations between the two sides of the equatorial Atlantic Ocean. Therefore, we do not further discuss West/Central African magmatism in this work. In summary, a total of 254 samples contributed to the geochemical characterization of the EQUAMP (Supplementary Data Table A1).

3.2. Self-Organizing maps

The SOM approach uses both competitive and cooperative learning processes to train "seed vectors" to represent patterns within the data to eventually be represented as "nodes" on the self-organized map. The output of the process is typically a two-dimensional "map" that essentially represents the total input (nD) dataset, with similar samples represented as "nodes" on the map, and the nodes themselves are ordered and positioned by their degrees of similarity or dissimilarity to each other. Because of the use of the vector quantization approach and measures of vector similarity, SOM modeling may be used to examine populations that are both Gaussian and non-Gaussian in nature and sample–variable relationships that are linear and/or nonlinear. Hence, the SOM process resembles a neural network (Kohonen, 1982, 2001; Fraser and Dickson, 2007; Friedel, 2011).

This study used the SiroSOM© package (Version 2.20.20190411.121434), an advanced computation tool developed by the Commonwealth Scientific and Industrial Research Organization (CSIRO). Parameters considered as input to a SiroSOM© analysis (apart from the data) include the size of the map described by the number of nodes as rows down (X) and the number of nodes as columns across (Y), which also dictates the total number of nodes used (i.e., $X \times Y$); the training length (number of iterations) for both the "rough" and "fine" cycles; and the shape of the search window with its initial and final sizes.

SiroSOM© offers analysis and "map" creation functions using either a rectangular (each node has 4 neighboring nodes) or hexagonal (each node has six neighboring nodes) lattice, with a sheet, cylinder or toroid serving as the projection surface used to transform from multidimensional (nD) space to 2D space. For instance, in the case of a toroid, the final 2D surface map is a flat surface with continuity (wrap-around) between opposite edges on the 2D map representation.

One advantage of the SOM approach is that the output "self-organized map" data can be visualized, displayed, or analyzed in many ways. The "unified distance matrix" or simply the U-matrix (Ultsch and Vetter, 1994), is a particularly useful 2D display, as it allows one to visualize patterns, similarities, and differences between the nodes in terms of Euclidean distances. Hence, one can visualize and interpret the relevance of natural domains or clusters within a dataset. Displaying the nodes using a color–temperature scale, for instance, with the color blue representing closeness between adjacent nodes and the color red representing dissimilarity or distance, would further enhance data visualization.

Component (plane) plots provide another 2D visualization of the "self-organized" map nodes that are particularly effective. These plots display, for each node, a plane or projection over a "map" that gives the contributions for any given variable (component) used in the analysis. Component (plane) plots can also be coded using a color–temperature scale, with blue nodes indicating a low contribution for a variable and red nodes indicating a high contribution. Another useful SOM output that is calculated and recorded for each input sample is the quantization error, which is ideally less than one, and the smaller the value is, the better. This error represents a measure of the distance between a sample and its representative node–vector.

If the user has a large dataset, the quantitative analysis of such data can be more readily facilitated by k-means (Davies and Bouldin, 1979) clustering of the SOM nodes (Vesanto and Alhoniemi, 2000). The estimation of the best number of clusters involves an unsupervised process calculated through the Davies––

Bouldin criterion (Davies and Bouldin, 1979) and considers the best subdividing scheme for each number of clusters in terms of Euclidean distances within and between the proposed numbers of clusters.

The similarity index in SiroSOM© is based on a cross-plot visualization of the first and second components of principal component analysis (PCA; Christophersen and Hooper, 1992). To gauge the correlations between the components (variables), this process involves a PCA followed by the display of the individual component planes on a PC#1 *versus* PC#2 cross-plot (using their calculated eigenvalue contributions). On this similarity index plot, components (variables) that are positively correlated parameters tend to plot closer together on one side of the diagram, whereas inversely correlated components tend to plot on opposing sides of the axes (García and González, 2004; Löhr et al., 2010).

In the processing of the PMP, EMP, and EQUAMP datasets on SiroSOM, we adopted an SOM map size of 58 (rows) × 52 (columns) with a total of 3,016 nodes. This map size was chosen to minimize the final quantization error and topologic error (both < 1). Unless indicated otherwise, the initialization (initiation, lattice, shape, and map size) and training parameters (neighbor, rough training, fine training, and errors) used to calculate the SOM computations are listed in the Supplementary Data Table A2. We must emphasize that the purpose of SOM use is not to replace expert petrological knowledge or to challenge previous geochemical classifications that are well established in these provinces. Rather, we use this approach to make a data-intensive regional comparison, since under the SOM method, it is possible to attribute an equal weight to all variables, as similarly concluded by Owen-Smith et al. (2021).

3.3. Geological mapping

The mapping of PMP, EMP and EQUAMP mafic rocks combines aeromagnetic data from the Geological Survey of Brazil (CPRM) and Bahia Mineral Research Company (CBPM), previous geological maps, and Google Earth images.

Because dikes are spread across a continent-scale area, each aeromagnetic survey was processed individually in Oasis montaj® (Geosoft). The geophysical data were previously corrected from diurnal variations and the International Geomagnetic Reference Field (IGRF). The processing routine was the same as that successfully used in part of the study area (de Castro et al., 2018; Melo et al., 2021, 2022). Geophysical processing started with a reduction to the magnetic pole (RTP) to correctly position the anomaly over its source. In addition, a pseudoinclination was applied to stabilize the results of this filter, followed by the amplitude of the analytical signal (ASA) to highlight the edges of magmatic bodies and directional enhancement filters applied to highlight magnetic anomalies that constitute dikes.

The magnetic map interpretations were compared with previously published geologic maps available in the database of the Geological Survey of Brazil and high spatial–temporal resolution Google Earth images to improve the mapping of mafic dikes. Linear (high-amplitude) magnetic anomalies commonly reflect shear zones, dikes, and regional faults. To sort out such ambiguities, we thoroughly assessed the anomalies, observing that dikes are represented on maps by strong positive and negative anomalies, with high amplitude in the ASA maps with well-marked orientations, and are usually arranged in swarms that are parallel to subparallel, forming *en echelon* geometries and frequently crosscutting the regional fabric at high angles. On the other hand, shear zones are structurally concordant with regional fabric, with magnetic anomalies being wider than those of dikes. Finally, regional faults may eventually stand out on magnetic maps, presenting a structural pattern similar to that of dikes, although fault anomaly patterns are discontinuous and more attenuated than those of both dikes and shear zones.

We additionally used GPlates 2.3.0 (https://www.gplates.org/) to manipulate plate reconstruction models and paleogeographic features of Early Cretaceous magmatism and South Atlantic-related hotspots through geological time. For this purpose, we assumed a stationary hotspot under a constantly moving plate. The results of this mapping work are shown in Fig. 1.

4. Results

4.1. Classification of the geochemical dataset

In the total alkali–silica (TAS) classification diagram (Fig. 2), the HT suite (TiO_2 > ~2 wt.%) of the PMP, EMP, and EQUAMP has SiO_2 < 56 wt.% and total alkalis ≤6.8 wt.%, plotting below the Miyashiro divisor (Miyashiro, 1978), with a few scattered samples falling above this line due to higher alkali/silica ratios. Consequently, HT compositions indicate subalkaline basalts, basaltic andesites, and basaltic trachyandesites. In the MgO *versus* TiO_2 diagram, the HT group clusters above the line defined by equation $TiO_2 = -0.1$ MgO + 3.3 for samples with MgO > 4 wt.%. For samples with MgO < 4 wt.%, the ascendant curve $TiO_2 = 0.725$MgO better separates the HT group from other suites. In the EQUAMP tholeiites, the Ti/Y parameter forms a continuous trend from 250 to 325, with overlaps between high- and low-Ti magmas. In Etendeka, Marsh et al. (2001) also reported difficulties in using the Ti/Y discriminator of Peate et al. (1992). Even so, HT presents high Ti/Y levels, usually above ~330, and is divided from other suites by the equation Ti/Zr = 0.4Ti/Y – 90 in the Ti/Y *versus* Ti/Zr plot. Incompatible elements are abundant (e.g., Sr > 400 ppm), and La/Yb > 10.

The ERs have SiO_2 content levels of 57–65 wt.% with TiO_2 < 2.5-wt.% and are mainly constrained within the trachyandesite–trachyte field (Fig. 2). In the Ti/Y *versus* Ti/Zr diagram, the plot of ER is similar to that of LT magmas in terms of Ti/Y, but ER has lower Ti/Zr levels. In terms of incompatible elements and REE contents, ER is akin to HT magmas (e.g., Sr > 400 ppm; La/Yb > 10). The stark contrast between ER and HT is perfectly identified by the influence of low TiO_2 content in conjunction with highly incompatible element amounts, as expected for fractionated rock. Previous petrological work on the PMP, EMP, and EQUAMP interpreted ER as AFC products derived from HT magmas (e.g., Florisbal et al., 2018; Macêdo Filho and Hollanda, 2022).

The LT (TiO_2 < 2 wt.%) magmas have lower alkali/silica ratios than HT rocks and are composed of subalkaline basalts and basaltic andesites, with a smaller group classified as andesite (Fig. 2) in the PMP and EMP. The LT tholeiites present low TiO_2/MgO and are thus arranged below the $TiO_2 = -0.1$MgO + 2.5 line in the MgO *versus* TiO_2 diagram for MgO > 3 wt.%. A particularity of the presence of PMP and EMP magmas is the presence of basalts to basaltic andesites with transitional TiO_2 content. Here, the transitional TiO_2 tholeiites (TTs) are those samples with TiO_2 levels of 2.7–1.7 wt.%. In the MgO *versus* TiO_2 diagram, TTs differ from the dominant HT and LT groups by clustering within the area defined by curves $TiO_2 = -0.1$MgO + 3.3 and $TiO_2 = -0.1$MgO + 2.5 (for MgO > 4 wt.% and 3 wt.%, respectively). However, in terms of incompatible element content, TTs are generally akin to the LT suites (i.e., Sr < 400 ppm; La/Yb < 10). In the EQUAMP, only a small number of samples plot within the TT field, but other geochemical parameters, such as trace elements and REEs, show that the samples belong to either the HT or LT groups. The LT and TT suites tend to plot above the curve defined by the equation Ti/Zr = 0.4MgO – 90 in the Ti/Y *versus* Ti/Zr diagram, controlled by low incompatible elements and REE contents. Notably, samples from False Bay and Saldanha Bay in southern Etendeka Province present a TiO_2 range

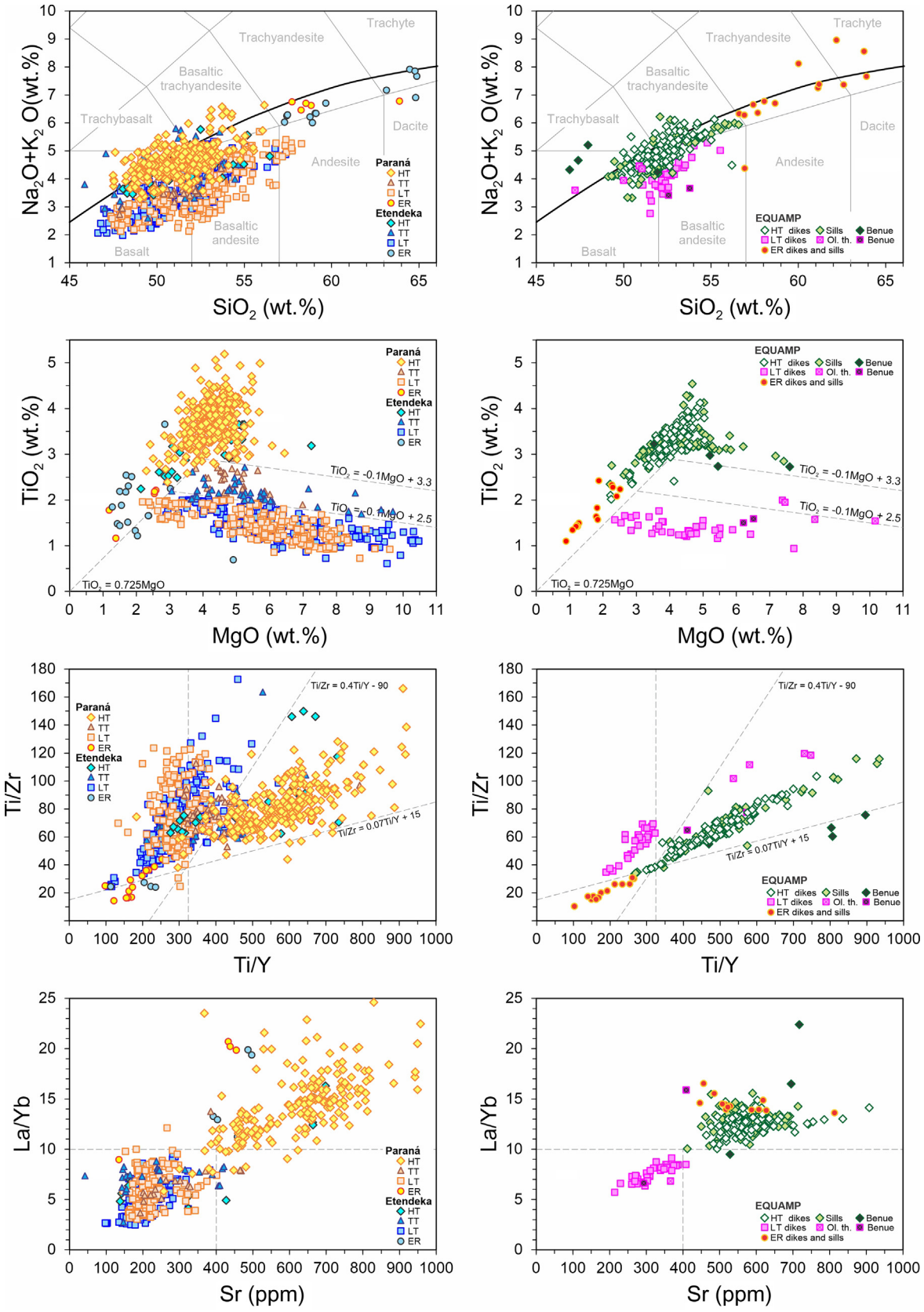

Fig. 2. Geochemical dataset of intrusive rocks of the Paraná, Etendeka and Equatorial Atlantic magmatic provinces used for SOM analysis. Samples are classified based on TiO_2 contents as high-Ti (HT), transitional-Ti (TT), and low-Ti (LT) tholeiites. A minor population of evolved rocks (ERs) is related to the evolution of mafic magmas by AFC processes. All bivariate plots consider LOI-free recalculation.

of 3.6–2.2 wt.% but low incompatible element levels compared to those observed in the LT tholeiites (Trumbull et al., 2007; Backeberg et al., 2011).

In an exploratory step, we evaluated the PMP, EMP, and EQUAMP datasets using PCA considering the whole-rock dataset of major oxides, trace elements (V, Cr, Co, Ni, Cu, Pb, Zn, R, Sr, Cs, Y, Zr, Nb, Ba, Hf, Ta, Th, and U) and REEs to reduce the dimensionality of the dataset and minimize information loss (Fig. 3). As shown in the PCA diagram for the EQUAMP (Fig. 3A), HT makes major contributions to Fe, Ti, P, Sr, HFSEs, and REEs. The ERs from the Rio Ceará-Mirim and Sardinha sills have a higher contribution of Si, alkalis (K and Na), and incompatible elements. The LT samples of the Rio Ceará-Mirim and Riacho do Cordeiro dikes show a strong correlation between them, plotting on the pole of samples depleted in trace elements.

The broad HT–ER geochemical groups of the EQUAMP plot together with the groups of the PMP and EMP, where the convex hull of the EQUAMP is completely included in the PMP and EMP range, which indicates analogous compositions for both domains (Fig. 3B). The LT samples of the EQUAMP are generally more evolved, plotting near the Al–Si-rich pole; nevertheless, the convex hull is completely inserted in the compositional range of the PMP and EMP (Fig. 3C). Moreover, TTs present a better correlation with the evolved LT group.

4.2. SOM approach

4.2.1. Component (plane) plots

An assessment of the component plots of the PMP, EMP, and EQUAMP (Fig. 4) shows that HT nodes have positive correlations with Fe_2O_3 and P_2O_5 and, to a lesser extent, with SiO_2, Na_2O, K_2O, MnO, and incompatible elements (Sr, Rb, Zn, Y, Nb, Ba, Zr, Hf, U, Th, Ta, and REEs) in a similar pattern, which is displayed by high P_2O_5 nodes. However, the latter P_2O_5 is better grouped with K_2O, Sr, Ba, Rb, and REEs. The low-TiO_2 nodes are distributed between the LT and ER groups, where LT magmas show positive correlations with MgO, CaO, and Al_2O_3 and to a lesser extent with Y, V, Ni, Cr, Co, and Cu, while ER is equivalent to high-SiO_2 nodes and positively correlated with Na_2O, K_2O, Rb, Y, Zr, Nb, Ba, Hf, Ta, Th, and REEs.

These observations are also supported by the similarity index based on PCA (PC1 *versus* PC2), where component plots of HFSEs, LILEs, and REEs have closer associations with high-TiO_2 and high-SiO_2 nodes (Fig. 5). The heavy REEs (HREEs) are grouped with Y, whereas light REEs (LREEs) are positively correlated with Zr, Hf, Ba, and Nb. Parameters such as $Fe_2O_3^T$ remain in an intermediate PC position and plot on the side of the diagram with incompatible elements, where its component plots together with other metals such as Mn, Zn, Cu, and V. The pole enriched in incompatible elements is better constrained by the HT and ER groups than by the LT group. Finally, the component plots of MgO, CaO, Al_2O_3, Ni, Cr, and, to a lesser extent, Co are interrelated in the TiO_2-poor pole of the PC plot.

4.2.2. Cluster analysis

When combining the PMP, EMP and EQUAMP datasets, the best K-means clustering yields 4 SOM-classified groups (Fig. 6; Table 2) for a Davies–Bouldin index value of 1.17: SA1, SA2, SA3, and SA4. Overall, the centroid values of clusters show strong contributions of MgO, CaO, K_2O, TiO_2, P_2O_5, and trace elements from four populations (Supplementary Data Table A3). However, Pb is a good discriminant only for the SA3 group, whereas Sr separates groups SA1 and SA2 from groups SA3 and SA4. The positions of the centroids of the four predefined geochemical groups plot close to the cluster centroids highlighted by the SOM analyses in the similarity index plot (Fig. 5), corroborating the strong correlation between the two classifications.

The SA1 cluster includes 83.2% of samples from the HT group. SA2 is characterized by 94.4% of ER compositions. Interestingly, this cluster groups magmas in a wider silica range (52–64 wt.%) than what was previously classified as ER (SiO_2 = 57–64 wt.%), assimilating 10.3% of the evolved HT samples. This means that SA2 should be a better indicator for separating basaltic andesitic–trachyandesitic fractionated samples from strict HT basaltic rocks. Cluster SA3 has a wide range of MgO from 3 wt.% to 10 wt.%, comprising 68.8% of all LT samples and 34.7% of TT tholeiites. On the other hand, SA4 comprises 58.7% of all TTs, followed by 30.3% of evolved LT compositions. In general, we observe that fractionation has a strong ability to modify the whole-rock geochemistry, which is well expressed in the HT–ER trend. Hence, cluster SA4 is produced from the strong similarity between evolved LT and evolved TT samples. Similarly, less evolved TT samples are allocated to SA3.

4.2.3. Trace element patterns

In Fig. 7, we evaluate those samples whose PMP, EMP, and EQUAMP petrological groups coincide with the SOM cluster analysis. Primitive mantle (PM)-normalized incompatible element diagrams (Sun and McDonough, 1989) show that the HT rocks in the PMP, EMP, and EQUAMP are very similar, displaying enrichment in LILEs over HFSEs and LREEs. The values for LILEs are approximately 30–270 times greater than the normalization parameters, while the HFSEs are enriched by factors of 15–75 (Fig. 7). The most striking differences between the provinces are related to Pb and Nb–Ta anomalies. The Pb anomalies are negative in the HT/SA1 cluster of the EQUAMP, whereas the PMP and EMP all groups tend to display positive spikes with a paucity of negative Pb anomalies. Nb–Ta anomalies are present in all provinces; however, in the EQUAMP, they tend to be uniform, generating an inverted trapezoidal pattern, while samples in the PMP and EMP present barely noticeable Ta anomalies.

The ER is enriched by 80–350 times the normalization parameters for LILEs and by 20–80 times for HFSEs but forms a distribution of incompatible elements akin to that of the HT group. Remarkable differences in comparison to mafic suites may be seen in LILE and HFSE enrichments coupled to prominent troughs at Ti–P; these features are completely plausible since high-Si magmas can be more enriched in incompatible elements. Moreover, P–Ti can diminish as a function of the fractionation of Fe–Ti oxides, pyroxenes, and apatite in parental tholeiitic melts.

The distribution of PM-normalized incompatible elements in LT magmas from the EQUAMP is homogeneous with marked negative Nb–Ta anomalies (also P and Ti) and positive Pb, La, Nd, and Zr–Hf anomalies. In PMP and EMP magmas, however, the greatest differences involve LILE contents that show heterogeneous behavior, varying by 7–200 times the normalization parameters, while HFSEs are <20-fold enriched. The large variation in LILE contents likely results from the high mobility of these elements.

4.2.4. Geographical distribution of magma types

Fig. 8 shows the geographical distribution of petrological groups and their respective comparisons with SOM clusters. In the PMP, SA1 (HT) occurs in the Transminas, Resende-Ilha Grande, Serra do Mar, and Florianópolis dike swarms and in central/northern Paraná sill complexes. In the EMP, SA1 (HT) is rare and occurs on the northern side of the main lava field and in the Angola area. In the EQUAMP, SA1 (HT) is the most common type found in both the Rio Ceará-Mirim dikes and Sardinha sills. SA2 (ER) is largely observed in association with SA1 (HT) in all three provinces. The LT types observed in SA3 and SA4 are the most common clusters in the southern PMP and EMP and are found in the

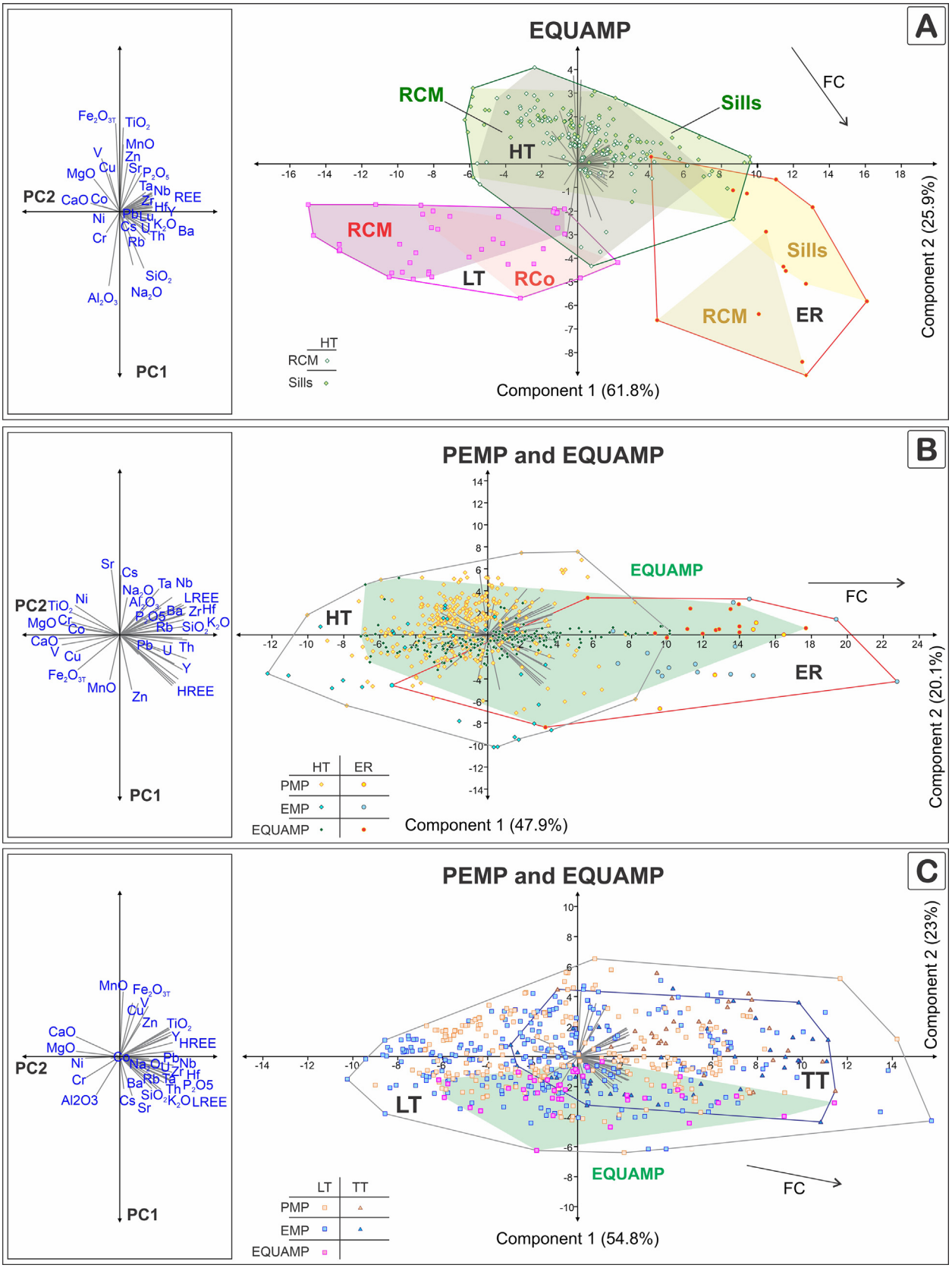

Fig. 3. Principal component analysis (PCA) plots. (A) PCA applied to the EQUAMP dataset: RCM (Rio Ceará-Mirim dikes), RCo (Riacho do Cordeiro dikes), and Sardinha sills. The high-Ti (HT) tholeiites and evolved rocks (ERs) of sills and dikes present comparable behavior, as similarly observed in low-Ti (LT) tholeiites of the RCM and RCo. (B) HT and ER from the combination of PMP, EMP and EQUAMP rocks. (C) LT and TT from a combination of PMP, EMP and EQUAMP rocks. Note that the EQUAMP convex hull is completely included in the convex hull of the Paraná-Etendeka Province (PEMP).

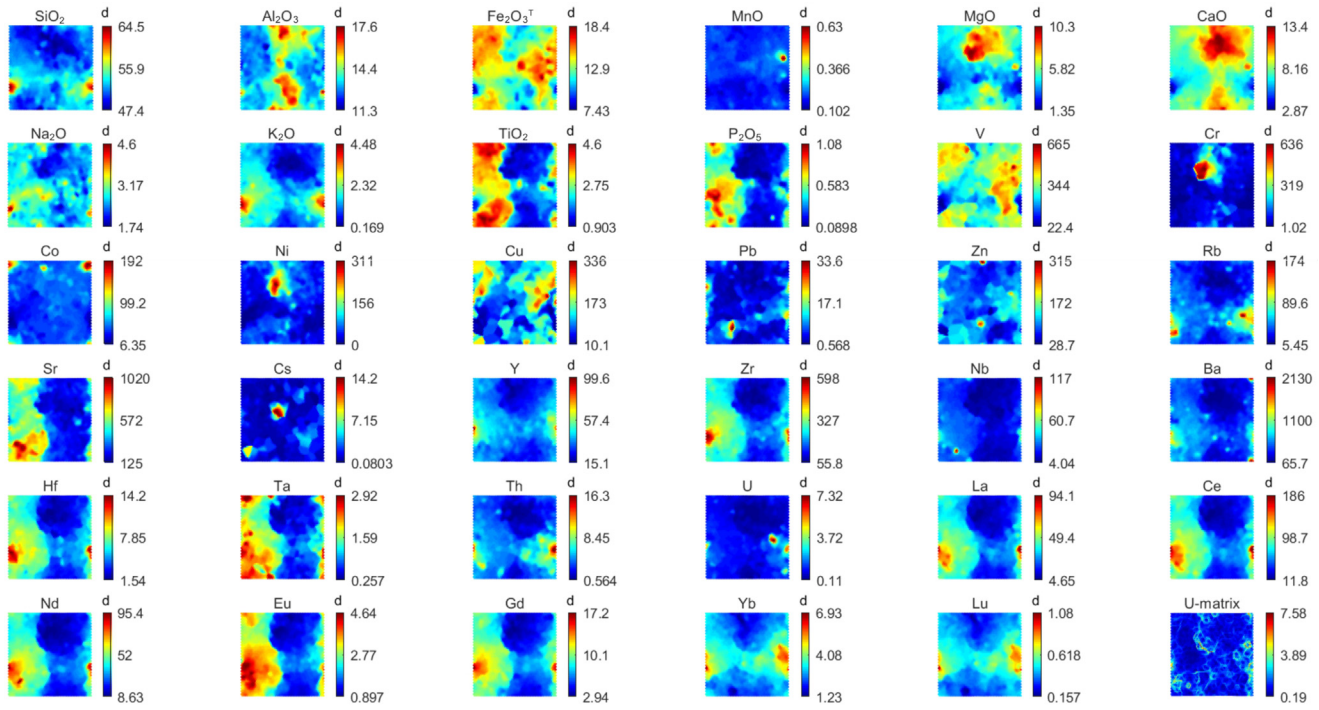

Fig. 4. Component plane plots for major oxides (wt.%), trace elements, REEs, and the U-matrix of the PMP, EMP and EQUAMP magmas. The numbers next to the color bars represent the maximum, average, and minimum values for each geochemical parameter. Some REEs are not shown, but they present component plane plots similar to those of neighbors.

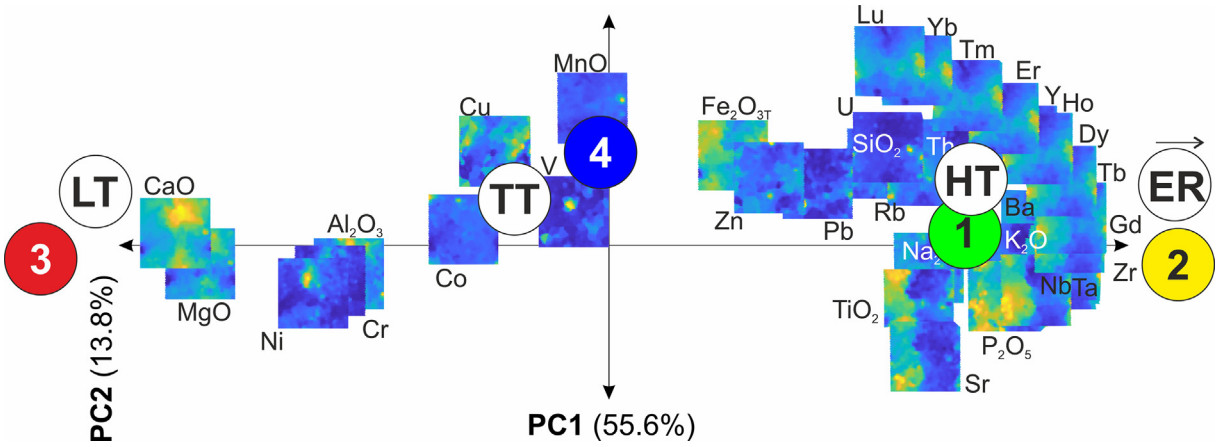

Fig. 5. Similarity index plot based on principal component analyses in SiroSOM for major oxides and trace and rare earth elements of the PMP, EMP and EQUAMP samples. The average positions of geochemical groups (HT, TT, LT, and ER) and clusters SA (1, 2, 3, and 4) are also represented.

Vitória-Colatina and Serra do Mar dike swarms. In the EQUAMP, the LT samples of the SA3 type occur at a single first-order dike at the intersection between the E–W Rio Ceará-Mirim and NE Rio Ceará-Mirim swarms and in the Riacho do Cordeiro dikes. The TTs of SA4 and SA3 are common only in the central PMP.

4.3. Radiogenic isotopes

In this section, isotopic relationships are exclusively explored according to intrusive systems based on geochemical groups. The Sr–Nd–Pb isotope ratios of the PMP, EMP, and EQUAMP dike swarms, sill complexes and Paraná basalt types (fields) are presented in Fig. 9. All Sr and Nd isotope-dependent parameters are recalculated to 130 Ma, which is considered an average age for Early Cretaceous magmatism in the South Atlantic area. However, Pb isotope compositions are plotted as present ratios since several published works do not measure Pb (or U, Th) concentrations, which precludes the correction for initial ratios. The references used are listed in the Supplementary Data Table A4.

The HT tholeiites of the PMP, EMP, and EQUAMP present high frequencies of $^{87}Sr/^{86}Sr_{(130\ Ma)}$ at ~0.705–0.706 (Fig. 9), and all samples have $\varepsilon_{Nd}(130\ Ma) < -1$. A few tholeiitic samples and ERs present a diffuse pattern toward radiogenic Sr, which may be suggestive of some degree of crustal assimilation. HT tholeiites of the Rio Ceará-Mirim dikes and Sardinha sills have high concentrations of $\varepsilon_{Nd}(130\ Ma)$ between −1 and −3, as do HT samples of the Florianópolis, Ponta Grossa, Resende-Ilha Grande, and southern Espírito Santo dike swarms. Another striking resemblance concerns HT tholeiites from the Bero volcanic complex in Angola/Etendeka Province, which shows the same Sr–Nd range as that

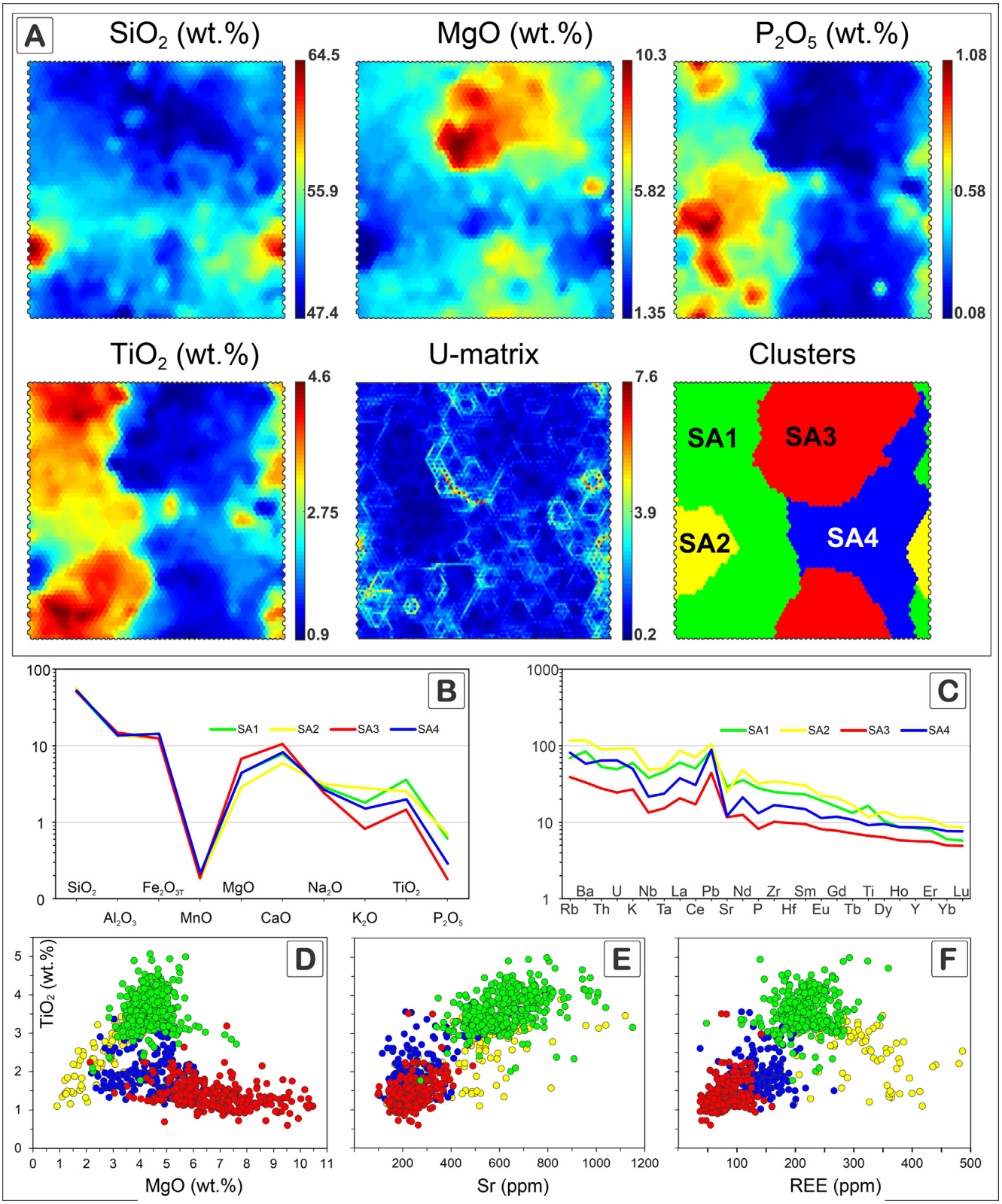

Fig. 6. Details of component plane plots of (A) SiO_2, MgO, P_2O_5 and TiO_2, U-matrix, and K-means clusters obtained by SiroSOM processing combining the PMP, EMP and EQUAMP: SA1, SA2, SA3, SA4. Spider plots represent the centroids of clusters for (B) major and (C) trace elements. Trace elements are normalized to the PM (Sun and McDonough, 1989). Clusters in (D) MgO *versus* TiO_2 diagram. (E) Sr *versus* TiO_2. (F) REE total *versus* TiO_2.

observed in the Rio Ceará-Mirim dikes and Sardinha sills. Moreover, the EQUAMP HT tholeiites plot over the HT Urubici/Khumib and Pitanga basalt fields for the PMP and EMP.

The LT tholeiites display a large range of Sr isotopes, forming a diffuse (fanlike) pattern, where less radiogenic Nd samples tend to show the most radiogenic Sr compositions. Such a

Table 2
Degrees of correlation among geochemical groups and K-means cluster analysis obtained in SiroSOM for the EQUAMP and PEMP.

Magma groups	*n*	Clusters			
		SA1	**SA2**	**SA3**	**SA4**
HT	561	**83.2 %**	10.3 %	1.24 %	5.2 %
ER	36	2.7 %	**94.4 %**	2.8 %	2.8 %
LT	542	0.2 %	0.7 %	**68.8 %**	30.3 %
TT	75	4 %	2.8 %	34.7 %	**58.7 %**

HT - high-Ti tholeiites; LT - low-Ti tholeiites; TT - transitional-Ti tholeiites; ER - evolved rocks; *n* - number of samples.

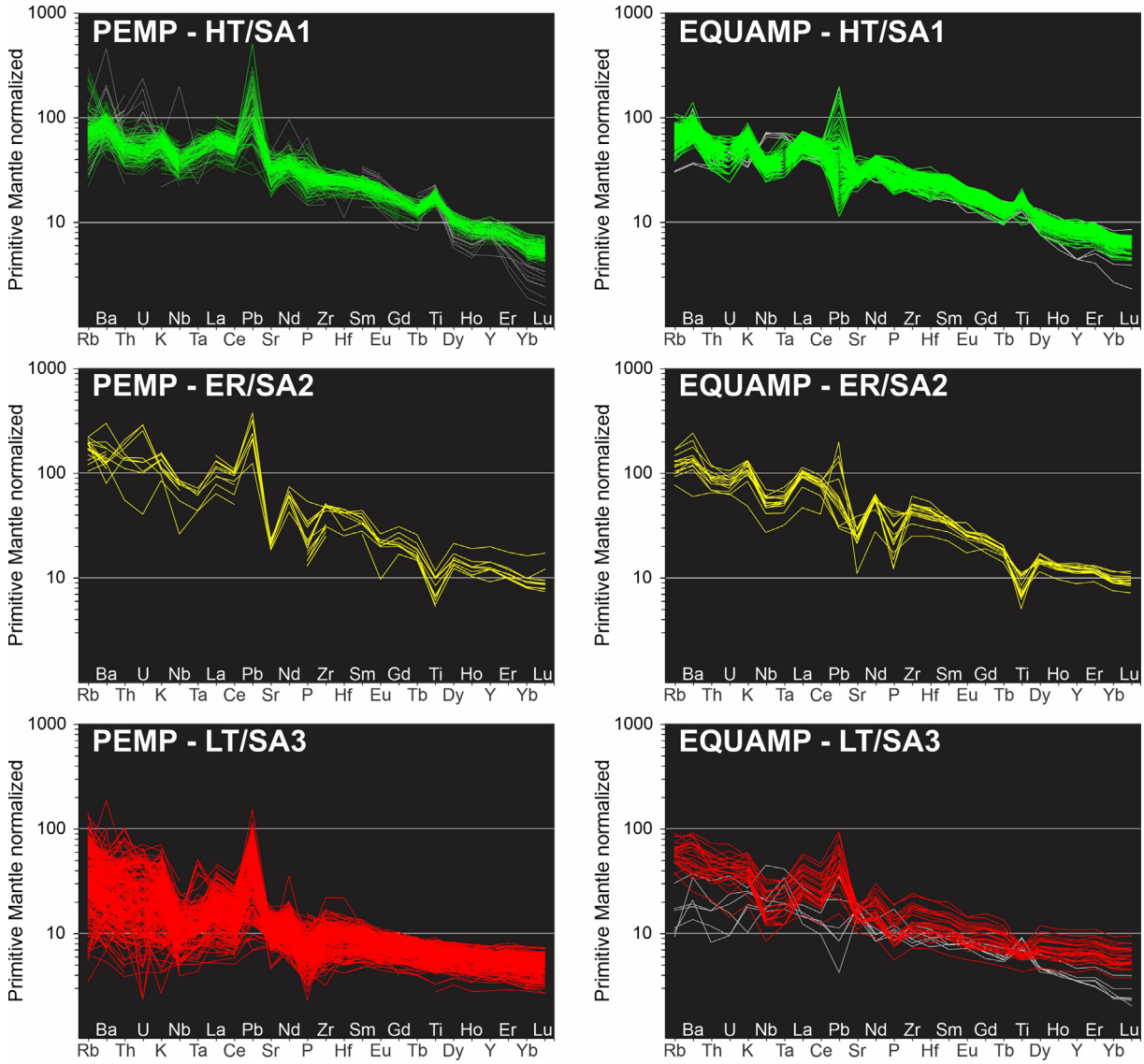

Fig. 7. Primitive mantle-normalized (Sun and McDonough, 1989) incompatible trace elements of the Paraná-Etendeka and Equatorial Atlantic (EQUAMP) provinces: high-Ti (HT) tholeiites in cluster SA1, evolved rocks (ERs) in cluster SA2 and low-Ti (LT) tholeiites in cluster SA3. Gray lines for the PMP and EMP are outlier samples, whereas in the EQUAMP diagrams, gray lines represent transitional basalts and olivine tholeiites of the EW-Rio Ceará-Mirim and northern Benue, which are plotted for comparison. SA4 is not shown because of its absent in EQUAMP and very heterogeneous pattern.

feature outlines a contamination trend toward lithospheric/crustal sources. The most primitive (asthenosphere-derived) samples concern the Henties Bay-Outjo, Möwe Bay, and Serra do Mar dikes, where ε_{Nd}(130 Ma) values concentrate between +1 and +6 coupled with $^{87}Sr/^{86}Sr_{(130\ Ma)}$ from 0.704 to 0.705. The second set of samples with $^{87}Sr/^{86}Sr_{(130\ Ma)}$ plotting from ~0.705 to 0.708 and ε_{Nd}(130 Ma) from +0.5 to −3.5 is observed in the Florianópolis, Ponta Grossa, Serra do Mar, Cedarberg, False Bay, and Möwe Bay areas, and samples showing less radiogenic Nd (ε_{Nd}(130 Ma) < −4) are diffuse. LT tholeiites of the Rio Ceará-Mirim and Riacho do Cordeiro have an isotopic signature (ε_{Nd}(130 Ma) < −4) similar to those of dikes from the Möwe Bay, Uruguay (Cuaró), southern Espírito Santo, and Vitória-Colatina and the Southern Paraná sills. Nonetheless, they still plot at the intersection between the fields of the Esmeralda and Gramado basalt types.

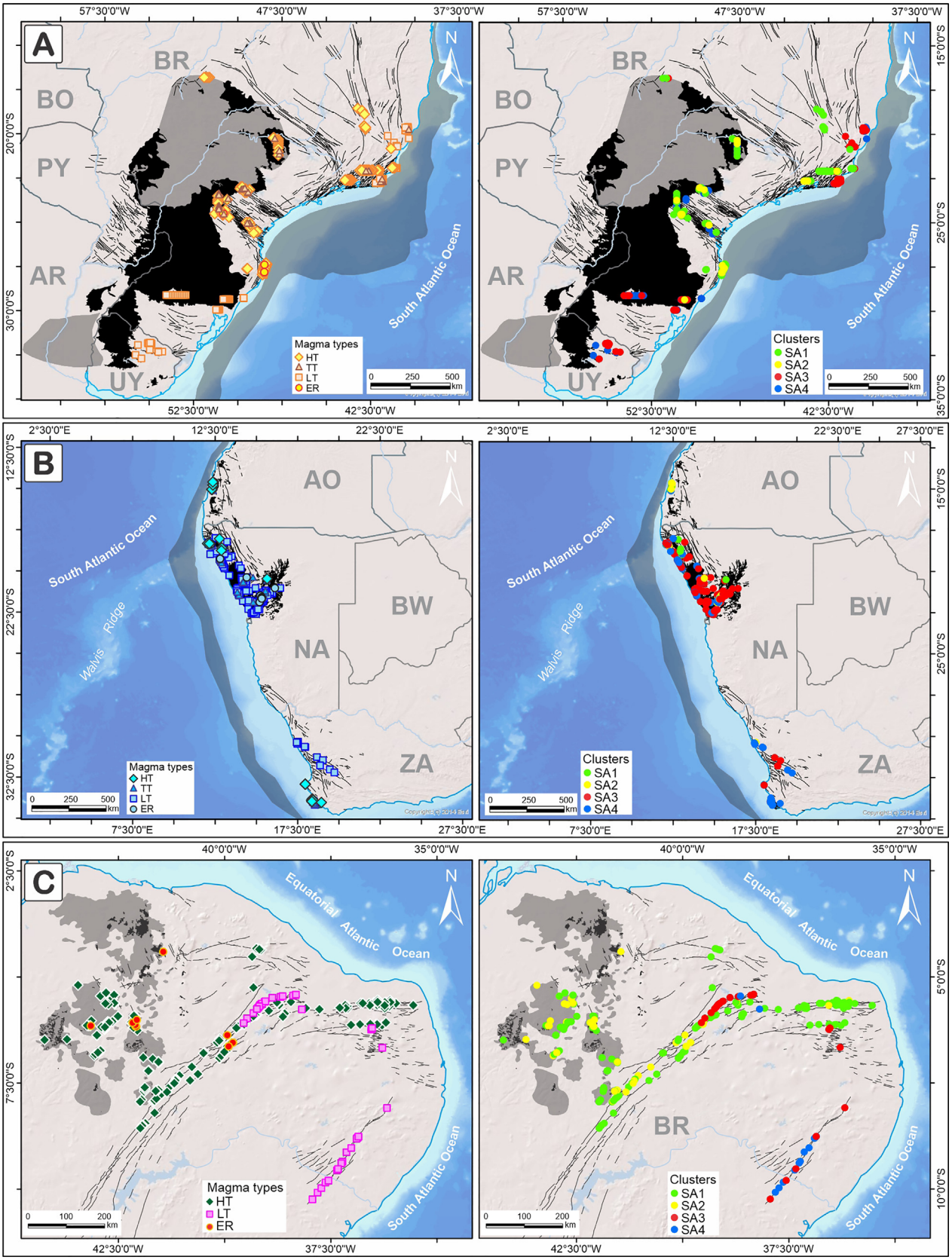

Fig. 8. Geographical distribution of magma groups and respective clusters obtained in the SOM solutions for the (A) Paraná, (B) Etendeka, and (C) Equatorial Atlantic provinces. Countries are represented by respective abbreviations: Brazil (BR), Argentina (AR), Uruguay (UY), Paraguay (PY), Bolivia (BO), South Africa (ZA), Namibia (NA), Angola (AO), and Botswana (BW).

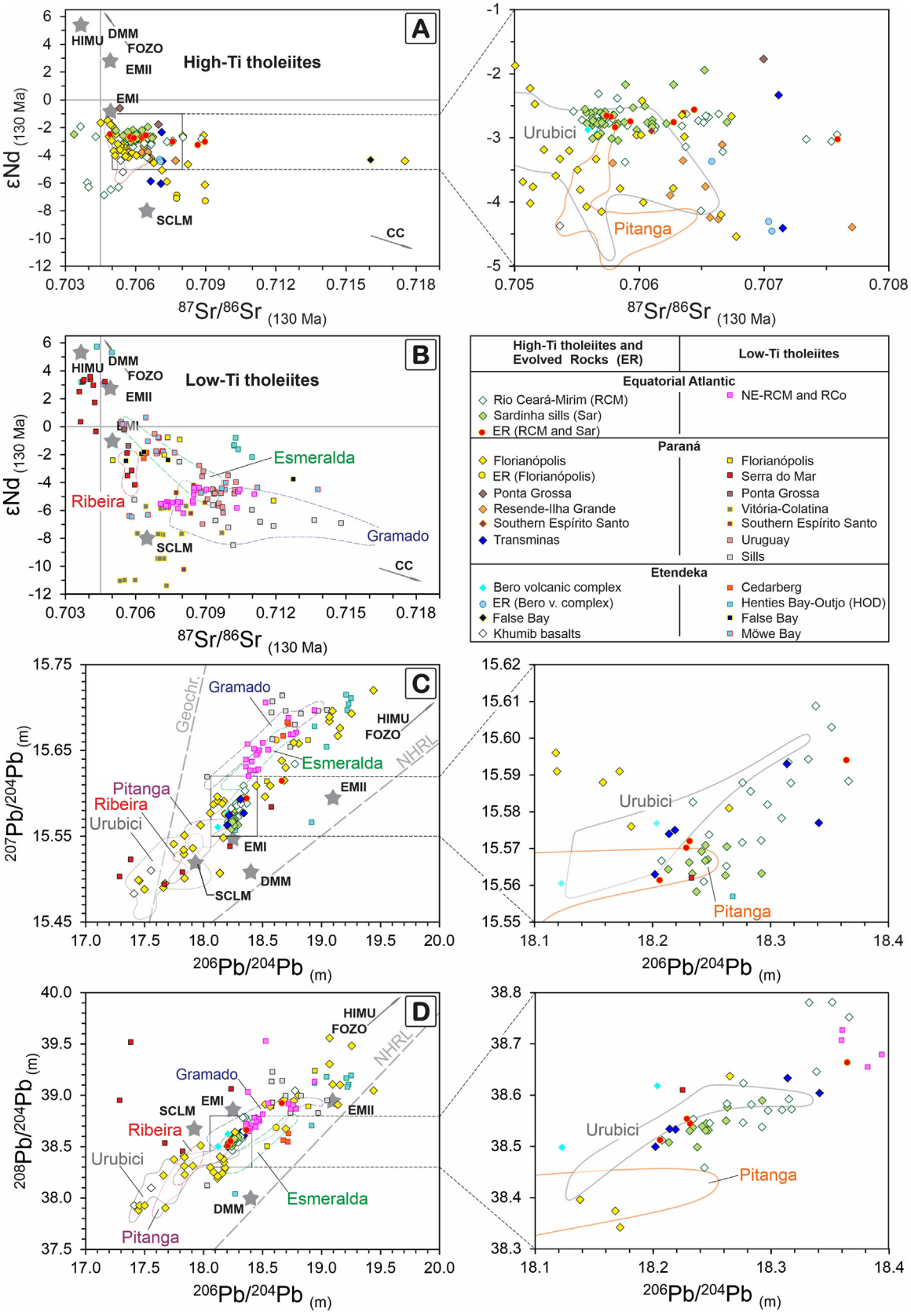

Fig. 9. Isotopic dataset (Sr, Nd, and Pb) of intrusive rocks from the Equatorial Atlantic, Paraná (with main basalt types plotted as fields) and Etendeka provinces. ε_{Nd}(130 Ma) *versus* $^{87}Sr/^{86}Sr_{(130\ Ma)}$ plots for (A) high-Ti and (B) LT. Intrusive forms and magma type fields are also represented in (C) $^{206}Pb/^{204}Pb_{(m)}$ *versus* $^{207}Pb/^{204}Pb_{(m)}$ and (D) $^{206}Pb/^{204}Pb_{(m)}$ *versus* $^{208}Pb/^{204}Pb_{(m)}$ plots and displayed in an adjacent closeup diagram. Centroid values of the mantle endmember were obtained from Stracke et al. (2005). The SCLM is represented by alkalic melts of Alto Paranaíba Province (Araujo et al., 2001). References of the isotope database are reported in the Supplementary Data Table A4.

Pb isotope data of samples from the PMP, EMP, and EQUAMP plot far above the Northern Hemisphere reference line (NHRL; Hart, 1984). The $^{206}Pb/^{204}Pb$ *versus* $^{207}Pb/^{204}Pb$ and $^{206}Pb/^{204}Pb$ *versus* $^{208}Pb/^{204}Pb$ diagrams (Fig. 9) support more radiogenic Pb compositions for LT tholeiites of the Rio Ceará-Mirim, Riacho do Cordeiro, Florianópolis, Cedarberg, Henties Bay-Outjo, and PMP sills, overlapping with the LT rocks of the Gramado and Esmeralda types. Exceptions are found for some LT samples from the Serra do Mar dikes with $^{206}Pb/^{204}Pb < 18$. In the HT group, less radiogenic Pb predominates, as observed in the Florianópolis, Urubici/Khumib and Pitanga basalts. The EQUAMP rocks exhibit most values of $^{206}Pb/^{204}Pb$ within an interval of ~18.2–18.4, which is also supported by narrow intervals of $^{207}Pb/^{204}Pb$ (~15.56–15.61) and $^{208}Pb/^{204}Pb$ (~38.50–38.80). These Pb isotope compositions are similar to those of several Florianópolis, Transminas, and Bero volcanic complex intrusions that plot within the Urubici/Khumib and Pitanga basalt fields. Broadly, a significant portion of HT-ER and LT rocks of the PMP, EMP, and EQUAMP plot around the enriched mantle components (mainly EMI).

5. Discussion

5.1. Ti-based classifications

The clustering results for the PMP, EMP, and EQUAMP exhibit a strong correlation with the Ti-based classification. In Fig. 10, we plot these data on different petrological/geochemical diagrams used to discriminate geochemical groups in the Paraná (Peate et al., 1992) and Etendeka mafic volcanic rocks (Marsh et al., 2001). Peate et al. (1992) proposed using a limit of TiO_2 at 2.8 wt.% to distinguish the Pitanga and Urubici basalts from the Paranapanema lavas. Licht (2018) proposed a cutoff at 2.8 wt.% TiO_2 to distinguish low- and high-Ti populations based on statistical gaps in frequency histograms. Overall, this limit is useful for HT rocks with MgO contents between 6 wt.% and 3 wt.%. Fractionated or slightly primitive types plot beneath or above this value, respectively. This limitation can be overcome by the combination of $TiO_2 = -0.1MgO + 3.3$ and $TiO_2 = 0.725MgO$ in the MgO *versus* TiO_2 plot, while the line defined by $TiO_2 = -0.1MgO + 2.5$ in the MgO *versus* TiO_2 binary plot can resolve ambiguities with HT and TT samples. In the diagram of Sr *versus* TiO_2, Marsh et al. (2001) proposed limits of 400 ppm and 2.2 wt.%, respectively, to separate HT and LT magmas. However, these straight limits exclude some Sr-poor HT types observed in other regions of the PMP and EMP. Therefore, we adopted the curve defined by $TiO_2 = -0.02Sr + 10$ as an alternative dividing limit between the HT and LT groups.

The Ti/Y *versus* Ti/Zr diagram has been extensively applied to the PMP and EMP magma classifications. Peate et al. (1992) proposed an arbitrary limit of Ti/Y < 310 to distinguish between HT and LT rocks, which worked well for flood basalts at the time. Nevertheless, the large amount of data produced indicates considerable overlap between the two broad groups. Moreover, the EQUAMP samples form a continuous trend from HT to ER. Herein, we prefer to use the curves defined by the equations $Ti/Zr = 0.4Ti/Y - 90$ and $Zr/Y = -0.045Ti/Zr + 9$ in the Ti/Zr *versus* Zr/Y and Ti/Zr *versus* Zr/Y plots, respectively, to minimize the overlap of magma compositions (Fig. 2). Another useful parameter for dividing HT and LT types is based on REE element abundances. For instance, the limit between the two broad groups concerning La/Yb ratios is usually defined at 10 (Fig. 2). Furthermore, high La/Yb values may be a proxy for the source (e.g., mantle rich in garnet), indicating that La is more compatible than Yb or may be indicative of less melting yielding mafic compositions with higher La/Yb levels (Greenough and McDivitt, 2018).

5.2. SOM solutions and previous classifications

The TiO_2 contents of HT/SA1 overlap with the compositions of Urubici/Khumib and Pitanga types in the PMP and EMP (Fig. 10). However, EQUAMP samples can plot beyond the limits defined by Urubici/Khumib and Pitanga. HT/SA1 presents very similar patterns in PM-normalized (Sun and McDonough, 1989) incompatible trace element diagrams, and isotopic data for Sr–Nd–Pb are much more cohesive. Therefore, HT rocks had the same/similar sources (or underwent similar petrogenetic processes) and a lower degree of contamination than those observed for the other groups. Nevertheless, the more dispersed behavior of the PMP and EMP tholeiites implies more important crustal contamination than in the EQUAMP. An indication of such a process is the ubiquitous positive Pb anomalies and comparative enrichments in LILEs.

The ER/SA2 in the EQUAMP and PMP magmas are interpreted as derived by AFC from HT types (Florisbal et al., 2018; Macêdo Filho and Hollanda, 2022). Some of the ERs from the EMP plots near LT types in the Zr/Y *versus* Ti/Zr diagram (Fig. 10). We are aware that these diagrams were developed to classify mafic types; thus, this behavior may even suggest that HT and LT tholeiites generate similar magma compositions after strong degrees of fractional crystallization. ERs are those with SiO_2 levels of 57–63 wt.%, but the SOM solutions classify intermediate rocks with $SiO_2 > 52.5$ wt.% as SA2. Intermediate compositions are typically assigned to types with SiO_2 levels of 52 – 63 wt.% (Le Maitre, 2002); therefore, SA2 can be a better means to separate andesitic rocks from strictly mafic melts (SiO_2 from 45 wt.% to 52 wt.%).

LT/SA3 generates a massive amount of data that overlap many petrological groups of Peate et al. (1992) and Marsh et al. (2001). In general, the Esmeralda and Gramado types are well correlated with LT types, and their broad classification as the LT group can be used if analysts are interested in simplistic models. However, when looking at PM-normalized (Sun and McDonough, 1989) incompatible trace element diagrams, it is possible to recognize a wide variety of behaviors with enrichment in LILEs, from those observed for lithosphere-influenced magmatism to flat patterns that resemble melts produced under high degrees of melting, such as E-MORB (Trumbull et al., 2007). Therefore, local predefined petrological groups play a role in the regional characterization of low-Ti types and diverse petrogenetic evolution. We should stress that many of these magmas underwent variable degrees of crustal assimilation processes, as suggested by isotopes, assimilating very heterogeneous crust/lithospheric mantle, which significantly modified the composition of the original magmas. This may even justify the fact that SOM solutions present less than a 70% correlation for LT types.

Finally, TT/SA4 presents $TiO_2 > ~2$ wt.% but is better correlated with LT melts than with HT types. In Paraná, Peate et al. (1992) proposed the Paranapanema (HT) and Ribeira (LT) groups to explain magmas with transitional Ti content. For intrusive forms and flood basalts, TTs are rare, and the limits proposed by Peate et al. (1992) overlap in several binary plots, leading to ambiguities. Overall, the trace element contents of TTs are akin to those of the LT group.

5.3. Timing of magmatic activity

The reported ages in Table 1 are presented as in their original papers. However, upon revising individual dates, large timing ranges can be observed for all provinces, mainly derived from poor interpretation of data, alteration or incorporation of excess radiogenic ^{40}Ar in K/Ar (and $^{40}Ar/^{39}Ar$) geochronology and other methodological issues (e.g., no report of decay constants, neutron flux parameters, criteria used for a plateau age). The accuracy and precision of published dates for the PMP and EMP have been

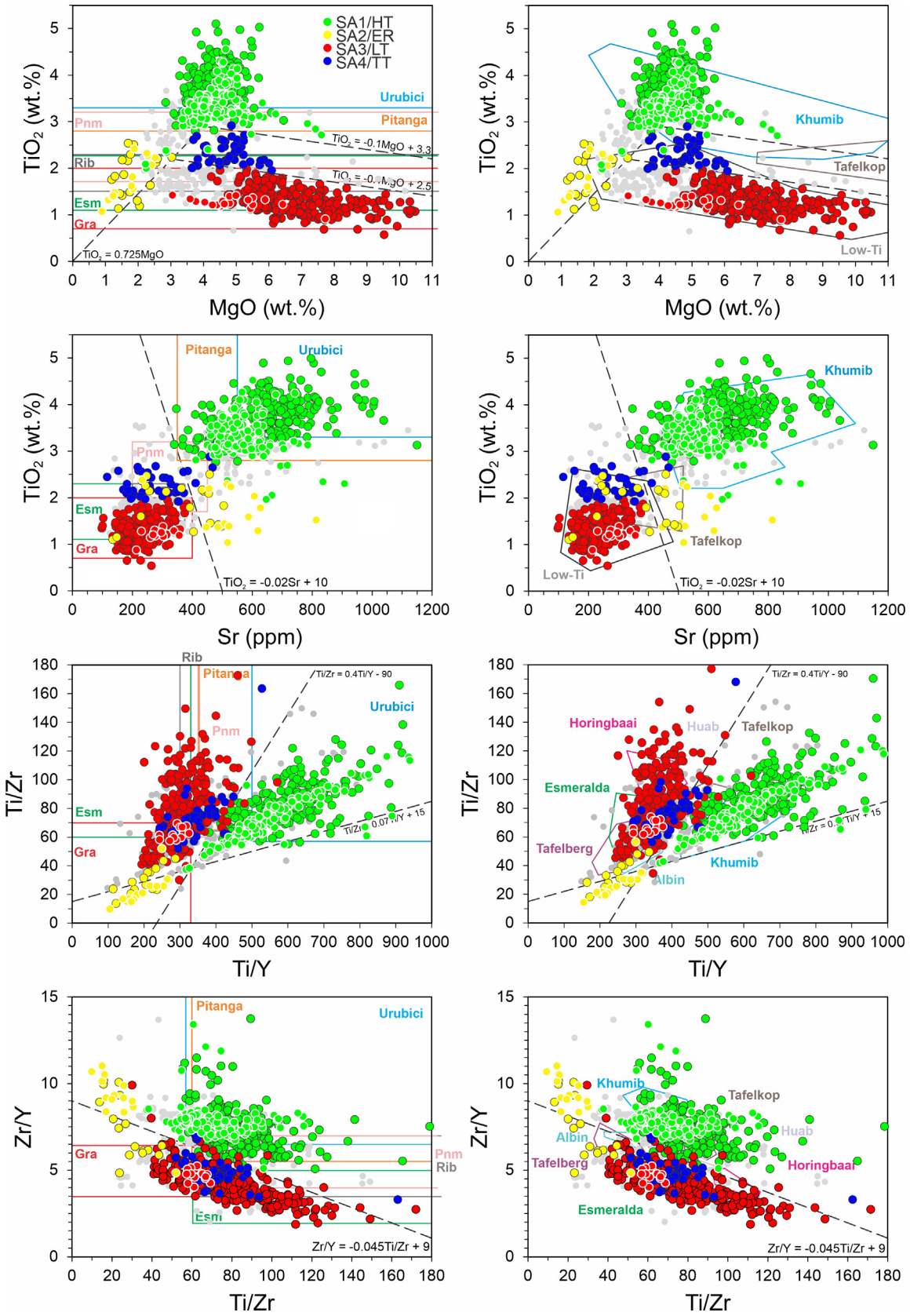

Fig. 10. Classification diagrams for mafic magma discrimination based on geochemical parameters for the Paraná-Etendeka province. Paraná magma types according Peate et al. (1992): Urubici, Pitanga, Paranapanema (Pnm), Ribeira (Rib), Gramado (Gra), and Esmeralda (Esm). Etendeka magma types cf. Marsh et al. (2001): Khumib, Talfelkop, Huab, Horingbaai, Talfelberg, and Esmeralda. Dots with white rims represent EQUAMP samples simplified as high-Ti (HT) tholeiites, low-Ti (LT) tholeiites and evolved rocks (ERs). Gray dots represent samples that do not exhibit correlations between clusters and Ti-based classification. Black dashed lines and respective equations represent proposed limits for dividing the broad compositional groups in the EQUAMP, PMP and EMP.

addressed by previous works, and a critical scrutiny of these dates indicates that the bulk magmatic activity of the PEMP is constrained to an interval of <3 Myr (Thiede and Vasconcelos, 2010; Gomes and Vasconcelos, 2021, and references therein). Thus, the actual timing (and the comparisons) of the magmatic activities of the provinces is derived solely on ages that pass the stricter validation parameter (Gomes and Vasconcelos, 2021). Therefore, we used the data filtering reported by Gomes and Vasconcelos (2021) for the PMP and EMP and applied similar parameters to the EQUAMP (Supplementary Data Table A5). These included reinterpretations of dates, recalculations of $^{40}Ar/^{39}Ar$ plateau ages (using the ArAr software; Mercer and Hodges, 2016) taking into account the new ^{40}K decay constant of Renne et al. (2011), and an FC sanidine age of 28.294 ± 0.036 Ma.

In the EQUAMP domains, the HT rocks constitute the major geochemical group, which is characterized by the consistency of $^{40}Ar/^{39}Ar$ ages (n = 10) within an interval from 133.5 ± 0.4 Ma to 126.4 ± 1.8 Ma, peaking at 130.4 Ma (Fig. 11) (Baksi and Archibald, 1997; Ngonge et al., 2016; Heilbron et al., 2018; Fernandes et al., 2020). One apparent outlier sample produced a younger date of 121.5 ± 0.8 Ma (Heilbron et al., 2018). In turn, the proposed PMP and EMP age intervals are grounded on at least sixteen times more date samples, and the emplacement timing of these provinces is set at an interval from 135.0 ± 0.6 Ma to 132.0 ± 0.2 Ma (Gomes and Vasconcelos, 2021). The main magmatic pulse is proposed based on an $^{40}Ar/^{39}Ar$ age peak of 134.5 Ma (Gomes and Vasconcelos, 2021) and zircon CA–ID (chemical abrasion–isotope dilution) TIMS U–Pb ages for the silicic volcanic rocks (Rocha et al., 2020). Considering only intrusive samples, the timing of the PMP and EMP is constrained mainly between 135.2 ± 1.4 Ma and 128.3 ± 0.8 Ma, with a main peak at approximately 130.4 Ma (Fig. 11).

Therefore, a coincidence of EQUAMP, PMP and EMP dates is evidenced by their overall coeval intrusive magmatic activities, where the major pulses are synchronous and the extrusive rocks of the PMP and EMP are apparently slightly older. This interval supports a short

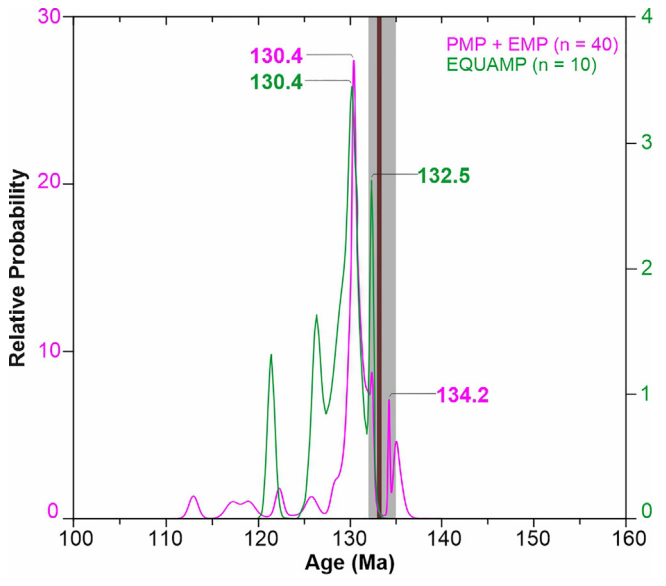

Fig. 11. Age probability plots based on recalculated (to the same decay constant and FC age) $^{40}Ar/^{39}Ar$ step-heating dates for the EMP and PMP (pink) (Gomes and Vasconcellos, 2021) and the EQUAMP (green) (Baksi and Archibald, 1997; Ngonge et al., 2016; Heilbron et al., 2018; Fernandes et al., 2020). The main age peaks are highlighted. The gray band represents extrusive rocks for the EMP and PMP combined (135.0 ± 0.6 Ma to 132.0 ± 0.2 Ma), and the brown band is the CA–ID TIMS zircon U–Pb age (133.66 ± 0.19 Ma to 132.72 ± 0.78 Ma) of Rocha et al. (2020) for the silicic volcanic rocks of the PMP. (For interpretation of the references to color in this figure legend, the reader is referred to the web version of this article.)

period of emplacement for Early Cretaceous tholeiitic magmatism in the South Atlantic realm, satisfying the geochronological criterion of LIPs (Ernst et al., 2021). Notwithstanding, the evident synchronicity in the three provinces reinforces their link as a single tectonic-magmatic event, which is imperative to understand how quickly the West Gondwana supercontinent breakup episode occurred.

5.4. Geodynamic models

LIP formation and emplacement have been the subject of extensive debate, in which the scientific community commonly evokes passive and active triggering mechanisms. For instance, some passive models envisage (i) upwelling of the hot asthenosphere beneath a lithosphere under stretching and thinning (e.g., White and McKenzie, 1989); (ii) thermal insulation beneath (super)continents (e.g., Coltice et al., 2007); (iii) edge-driven convection (e.g., King and Anderson, 1995); or (iv) delamination of the thickened lithosphere and consequent ascent of the asthenosphere triggering melting of the eroded lithosphere left behind (e.g., Seber et al., 1996). Conversely, active models assume the involvement of a mantle plume at the base of the lithosphere causing regional uplift, rifting and volcanism (e.g., Wilson, 1973; Ernst and Buchan, 1997).

In recent decades, plume theory has gained strength since global tomographic models have shown a clear concurrence among eruption sites of LIPs and marginal areas of large low shear-wave-velocity provinces (LLSVPs) (Fig. 12) existing beneath Africa and the mid-Pacific Ocean (Torsvik et al., 2006; Svensen et al., 2018). The Tristan-Gough hotspot has been one of the most invoked mechanisms to explain anomalous igneous activity in the South Atlantic realm (e.g., Courtillot et al., 2003). Accordingly, the drifting of West Gondwana over the African LLSVP transported the Namibia/Angola area to the Tristan-Gough plume at 135.0 ± 0.6 Ma (Heit et al., 2015; Ryberg et al., 2015; Matthews et al., 2016), where it caused regional uplift (Cox, 1989; Krob et al., 2020), extensive tectonics and the initial eruptive stage of the Paraná-Etendeka event (Gomes and Vasconcelos, 2021).

Svensen et al. (2018) envisage a long-lived Andean subduction process as the triggering mechanism for a deep plume rising from the African LLSVP border that led to the emplacement of the Paraná-Etendeka event. Indeed, shallow mantle melting models (e.g., edge-driven convection or thermal insulation) do not support near-synchronous voluminous melt production over transcontinental distances in West Gondwana. In contrast, current geological evidence shows remarkable offshore Cretaceous magmatism, in addition to a well-developed hotspot track (Tristan-Walvis Ridge), leading to the focal region of the Paraná-Etendeka LIP in Africa (e.g., Rohde et al., 2013; Homrighausen et al., 2019). Moreover, high-temperature basalts/picrites are virtually absent in the PMP and EQUAMP, but they are common in the EMP (e.g., Trumbull et al., 2004, 2007; Keiding et al., 2011, 2013; Stroncik et al., 2017). All these findings suggest that if a plume was active in the pre-South Atlantic area, it might be reasonably located beneath Africa.

Nevertheless, the geochemical contribution of the Tristan hotspot as the source of the Paraná-Etendeka basalts has been questioned in the literature because the Tristan member does not resemble the Paraná-Etendeka melts (e.g., Rocha-Júnior et al., 2012). Alternatively, most Sr–Nd–Pb isotope data for the PMP and EMP overlap the fields of the Gough-EMI member (Hoernle et al., 2015). Rohde et al. (2013) observed bilateral chemical zonation between the Tristan and Gough tracks traced for 70 Ma; consequently, the Tristan-Gough plume was a single hotspot pervasively EMI-Gough flavored during the Early Cretaceous. Peate et al. (1999) and Gibson et al. (2005) explained Gough-EMI characteristics with delaminated subcontinental lithospheric mantle (SCLM) mixed with plume components (e.g., FOZO). In a recent view, Hoernle et al. (2015) proposed a deep plume source derived

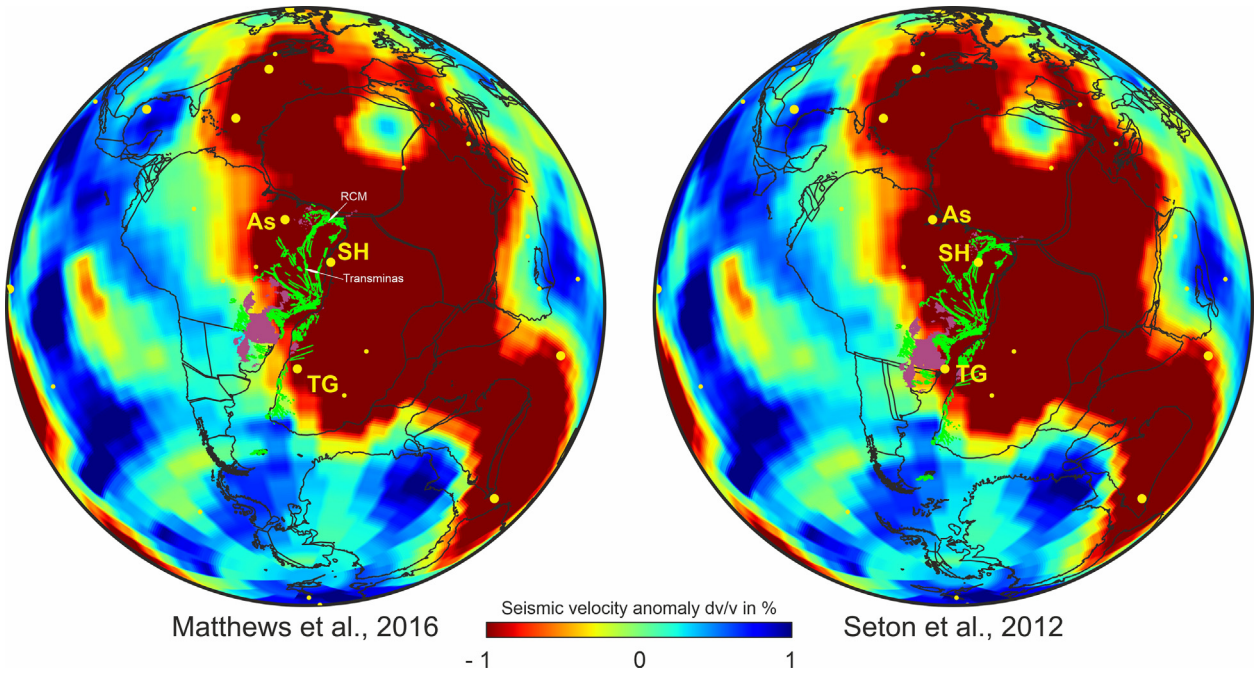

Fig. 12. Tomographic slice at 2800 km depth beneath the South Atlantic Ocean region (TX2019slab-s model; Lu et al., 2019) combined with a plate reconstruction model at 134 Myr (Seton et al., 2012; Matthews et al., 2016). The high-temperature colors (brown to red) indicate the African/Tuzo LLSVP (Large Low-shear Velocity Province). Early Cretaceous igneous provinces are represented as dikes (green traces), sills and floods (purple polygons). Hotspots are represented as yellow dots with respective acronyms: Tristan-Gough (TG), Saint Helena (SH), and Ascension (As). Seismic tomography and plate reconstruction models were generated using SubMachine tools (Hosseini et al., 2018). (For interpretation of the references to color in this figure legend, the reader is referred to the web version of this article.)

from the African LLSVP margin to explain the Gough-EMI type in the Southern Atlantic area (see, also, Homrighausen et al., 2019), which subsequently mixed with lithospheric components to form the Paraná-Etendeka basalts.

Overall, LT dikes of the PMP, EMP, and EQUAMP outline a major role in lithospheric assimilation, which is reinforced by increases in $^{87}Sr/^{86}Sr_{(130\ Ma)}$ accompanied by decreases in MgO and $^{143}Nd/^{144}Nd_{(130\ Ma)}$. This evidence corroborates works that evoke lithospheric mantle and/or mixing of the enriched SCLM with depleted mantle sources plus some crustal contribution to form LT types (e.g., Trumbull et al., 2007; Muzio et al., 2017; Marques et al., 2018; Pearce et al., 2021). Asthenosphere-derived melts have been identified in Henties Bay-Outjo tholeiites, for which Trumbull et al. (2007) interpreted enriched mid-ocean ridge basalt (E-MORB) as the primary source. Notably, E-MORBs are classically formed in areas where there is some interaction between a depleted upper mantle and enriched material (e.g., mantle plume; Schilling et al., 1985). In the PMP, isotopically depleted melts are identified in the Serra do Mar dikes (Almeida et al., 2021; Carvas et al., 2021), which were mostly emplaced in the coastal area projected toward Africa in a pre-breakup context. Therefore, an asthenospheric component such as MORB (or even E-MORB) might be reasonably considered as the parental source of low-Ti magmas. In this case, low-Ti melts would require considerable assimilation of heterogeneous lithospheric components to explain the compositional/isotopic diversity. For instance, Precambrian components from West Gondwana have been adopted as contaminant representatives in AFC models for the Paraná, Etendeka and EQUAMP tholeiites (e.g., Peate et al., 1999; Hoernle et al., 2015; Oliveira et al., 2018; Marques et al., 2018; Beccaluva et al., 2020; Macêdo Filho and Hollanda, 2022).

A plausible model triggered by plume impingement (Fig. 13A) should be outlined if the upper asthenosphere melted (DMM) and mixed with a minor plume component (OIB) to form an E-MORB member (Macêdo Filho and Hollanda, 2022). In a nonplume model (Fig. 13B), the SCLM-derived melts might be the enrichment agent of DMM to form E-MORB. These hotter and magnesian E-MORB magmas would be subsequently contaminated with lithospheric materials while fractionating and upwelling through the crust to generate the wide geochemical-isotopic range observed in low-Ti tholeiites (Beccaluva et al., 2020). If an OIB-EMI plume is elected as a source of the HT group (Fig. 13A), only a small degree of lithospheric/crustal assimilation is required to explain the HT isotopic diversity (Macêdo Filho and Hollanda, 2022), in agreement with De Min et al. (2018) and Pearce et al. (2021). Otherwise, in a nonplume model, Macêdo Filho and Hollanda (2022) envisage a DMM source assimilating 10%–20% enriched SCLM-derived melts with minor involvement of continental crust to form the EMI-flavored HT type (Fig. 13B).

The 134 Myr reconstruction model of Seton et al. (2012) located the Tristan-Gough plume head near the Florianópolis dikes (Fig. 12). This swarm is commonly taken as the feeder system of the Urubici/Khumib basalts in the PMP and EMP (Peate et al., 1999; Florisbal et al., 2018; McMaster et al., 2019). Another mantle plume model in South America was proposed by VanDecar et al. (1995), who identified a Tristan-Gough hotspot in SE Brazil. Curiously, the Ponta Grossa, Serra do Mar, and NW-Transminas dike swarms suggest a circumferential/elliptical pattern surrounding the VanDecar's plume fossil conduit (Fig. 1). On the other hand, many dike swarms seem to radiate from the Namibian/Angolan coast (Fig. 1), where evidence of plume impingement has been reported in the literature (e.g., Ryberg et al., 2015).

As we can see, there is no consensus on the exact location of the plume center beneath West Gondwana, but most works agree that if it was present, it was somewhere between the Namibia/Angola and South American counterparts. Thus, assuming that the source of tholeiitic magmas is in the southern Atlantic, the distal (and slightly younger?) magmatic manifestations of South America, such as those of the EQUAMP, might represent remnants of effective plumbing systems able to transport magmas over long distances. A remarkable indication of this physical linkage is the

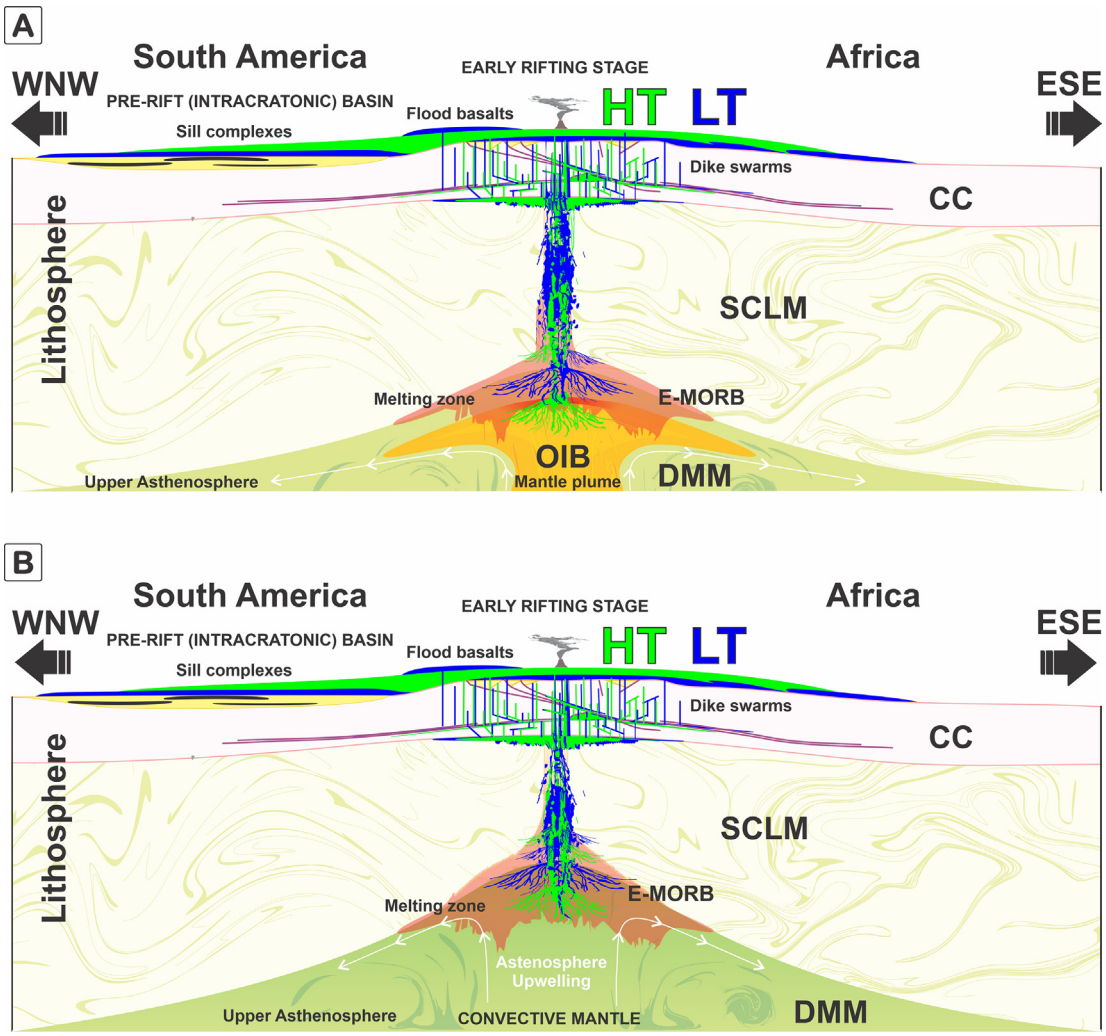

Fig. 13. Schematic illustration with examples of (A) active and (B) passive triggering mechanisms of LIPs. (A) Model of a mantle plume as a partial source of magmatism, where LT magmas would have been generated by the mixing of asthenospheric mantle melts (DMM; depleted MORB mantle) with enriched lithospheric mantle-derived melts (SCLM; subcontinental lithospheric mantle) and subsequently contaminated with crustal materials (CC; continental crust). Magmas rich in incompatible elements, such as HT magmas, in turn would be explained by an OIB (EMI) derived from a mantle plume with some assimilation of lithospheric materials. In (B), in a passive asthenosphere upwelling mechanism, asthenosphere-derived melts (DMM) variably mixed with lithospheric components (SCLM + CC) were the source of tholeiitic magmatism.

Rio Ceará-Mirim and Transminas mega-swarm, forming a suggestive single plumbing system up to 2,300 km long (Macêdo Filho and Hollanda, 2022). Similar correspondence exists between Early Cretaceous low-Ti dikes of the Riacho do Cordeiro and Vitória-Colatina swarms that are inferred from magnetic anomalies of at least 1,600 km arranged parallel/subparallel to the adjacent South Atlantic Ocean margin (Fig. 1).

Expanding these correlations to other intrusive components, at least in eastern South America, the dike swarms related to the South Atlantic margin are dispersed in a contiguous area c. 4000 km long, characterizing one of the largest sets of tholeiitic plumbing systems on Earth. In this context, the EQUAMP integrates the framework of Early Cretaceous provinces forming together with the PMP and EMP a major single LIP related to the early opening stage of the South Atlantic Ocean. Considering this scenario, a more appropriate name to refer to these three provinces in conjunction is the South Atlantic Magmatic Province (SAMP). Thus, the diachronic opening of the Atlantic Ocean would be simplified and fully explained by breakup/magmatic events registered by the Central Atlantic (Jurassic-Triassic), South Atlantic (Early Cretaceous, including the equatorial margin representatives), and North Atlantic (Paleogene) magmatic provinces.

6. Conclusions

A re-evaluation of databases from the PMP, EMP and EQUAMP allowed us to draw the following brief conclusions:

(1) The high-Ti tholeiites of the Rio Ceará-Mirim, Canindé and Sardinha sill complexes present identical geochemical–isotopic–geochronological aspects. Analogous conditions are observed among the low-Ti magmas of the Rio Ceará-Mirim and Riacho do Cordeiro swarms. Such findings support the proposal of a single intrusive LIP in NE Brazil (EQUAMP).
(2) Irrespective of the data analysis tools adopted, whether involving conventional classifications (petrological skills) or unbiased machine learning-based approaches (PCA; SOM), the results indicate strong geochemical–isotopic–geochronological equivalences of EQUAMP intrusions with several plumbing systems reported in the PMP and EMP (e.g., Florianópolis, Ponta Grossa, Resende-Ilha Grande, Southern Espírito Santo, Transminas, and Bero intrusions).
(3) The physical connection between the high-Ti dikes of the Rio Ceará-Mirim and Transminas swarms is feasible and reinforced by geochemical–isotopic–geochronological data

(Macêdo Filho and Hollanda, 2022). Similar understandings may be outlined for the low-Ti dikes of the Riacho do Cordeiro (EQUAMP) and Vitória-Colatina swarms (PMP).

(4) Based on a multidata assessment, the EQUAMP, PMP and EMP should be grouped to form a single intercontinental-scale tholeiitic event related to the early stage of the South Atlantic opening during the Early Cretaceous.

(5) In prebreakup reconstructions, the extension of this widespread magma input is dispersed from the West/Central African rift system to the Falkland Islands/South Africa (>6000 km), composing one of the largest LIPs on Earth (i.e., $\sim 10 \times 10^6$ km^2), not only in terms of the volume of flood basalts but also in terms of the area of intrusive remnants.

(6) The early stages of continental breakup and consequent genesis of the Atlantic Ocean in its entirety are recorded (and simplified) into three major tectonic/magmatic events: Jurassic–Triassic/CAMP, Early Cretaceous/SAMP and Paleogene/NAMP.

Declaration of Competing Interest

The authors declare that they have no known competing financial interests or personal relationships that could have appeared to influence the work reported in this paper.

Acknowledgments

A.A. Macêdo Filho acknowledges the Brazilian agencies FAPESP (2017/13130–0) and CAPES (1643026) for the PhD scholarships at the USP and the Research Internships Abroad Program (BEPE/FAPESP) for the scholarship at the UQ (2018/24769–5). A.A. Macêdo Filho also thanks the BRC team for the friendly support during the period at the SMI/UQ. M.H.B.M. Hollanda, A.L. Oliveira, and A. Dantas are grateful to the CNPq for the research fellowship (303201/2019-3), PhD scholarship (141413/2018-2), and MSc scholarship (132996/2019-7) at USP, respectively. A.C.C. Melo thanks the CAPES for the sandwich PhD scholarship at the UQ (88881.188664/2018-01). We would like to thank the CSIRO (AUS) for providing an updated SiroSOM license during the early stage of this research. We acknowledge R. Damian Nance (science editor), Allan Gomes, Michael McMaster, and three other anonymous reviewers for constructive comments that considerably helped us improve this manuscript. This article is part of A.A. Macêdo Filho's PhD dissertation (Macêdo Filho, 2021) and corresponds to contribution No. 7 for the EQUAMP project (FAPESP 2017/08429-9).

Appendix A. Supplementary data

Supplementary data to this article can be found online at https://doi.org/10.1016/j.gsf.2022.101479.

References

Almeida, J.C.H., da Costa, P.L., Heilbron, M., Da Silva Schmitt, R., De Morisson Valeriano, C., Rubim, I.N., Mohriak, W.U., Júnior, D.L.M., Tetzner, W., 2013b. Guia de campo na Área Continental do Alto de Cabo Frio. Bol. Geoc. Petrobras 21, 325–355 (in Portuguese).

Almeida, J., Dios, F., Mohriak, W.U., Valeriano, D.M., Heilbron, M., Eirado, L.G., 2013a. Pre-rift tectonic scenario of the Eo-Cretaceous Gondwana break-up along SE Brazil – SW Africa: insights from tholeiitic mafic dyke swarms Pre-rift tectonic scenario of the Eo-Cretaceous Gondwana break-up along SE Brazil – SW Africa: insights from tholeiitic mafic dyke swarms. Geol. Soc. London Spec. Pub. 369 (1), 11. https://doi.org/10.1144/SP369.24.

Almeida, J., Heilbron, M., Guedes, E., Neubauer, F., Manfred, B., Klausen, M.B., Valeriano, C.M., Bruno, H., Giro, J.P., McMaster, M., Tetzner, W., 2021. Pre-to-syn-rift tholeiitic magmatism in a transtensive hyperextended continental margin: Onshore and offshore magmatism of the Campos Basin, SE Brazil. J. S. Am. Earth Sci. 108,. https://doi.org/10.1016/j.jsames.2021.103218 103218.

Almeida, V.V., Janasi, V.A., Heaman, L.M., Shaulis, B.J., Hollanda, M.H.B.M., Renne, P. R., 2018. Contemporaneous alkaline and tholeiitic magmatism in the Ponta Grossa Arch, Paraná-Etendeka Magmatic Province: Constraints from U-Pb zircon/baddeleyite and ^{40}Ar/^{39}Ar phlogopite dating of the José Fernandes Gabbro and mafic dykes. J. Volcanol. Geotherm. Res. 355, 55–65. https://doi.org/10.1016/j.jvolgeores.2017.01.018.

Araujo, A.L.N., Carlson, R.W., Gaspar, J.C., Bizzi, L.A., 2001. Petrology of kamafugites and kimberlites from the Alto Paranaíba Alkaline Province, Minas Gerais, Brazil. Contrib. Mineral. Petrol. 142 (2), 163–177. https://doi.org/10.1007/s004100100280.

Backeberg, N.R., Reid, D.L., Trumbull, R.B., Romer, R.L., 2011. Petrogenesis of the false bay dyke swarm, Cape Peninsula, South Africa: evidence for basement assimilation. S. Afr. J. Geol. 114 (3–4), 335–352. https://doi.org/10.2113/gssajg.114.3-4.335.

Baggio, S.B., Hartmann, L.A., Lazarov, M., Massonne, H.J., Opitz, J., Theye, T., Viefhaus, T., 2018. Origin of native copper in the Paraná volcanic province, Brazil, integrating Cu stable isotopes in a multi-analytical approach. Miner. Depos. 53, 417–434. https://doi.org/10.1007/s00126-017-0748-2.

Baksi, A.K., Archibald, D.A., 1997. Mesozoic igneous activity in the Maranhão Province, Northern Brazil - ^{40}Ar/^{39}Ar evidence for separate episodes of basaltic magmatism. Earth Planet. Sci. Lett. 151, 139–153. https://doi.org/10.1016/S0012-821X(97)81844-4.

Beccaluva, L., Bianchini, G., Natali, C., Siena, F., 2020. Plume-related Paranà-Etendeka igneous province: An evolution from plateau to continental rifting and breakup. Lithos 362–363,. https://doi.org/10.1016/j.lithos.2020.105484 105484.

Belém, J., 2014. Geoquímica, Geocronologia e Contexto Geotectônico do Magmatismo Máfico Associado ao Feixe de Fraturas Colatina, Estado do Espírito Santo. PhD thesis. Universidade Federal de Minas Gerais, Belo Horizonte, Brazil, 134 p (in Portuguese).

Bellieni, G., Comín, P., Marques, L., Melfi, A., Piccirillo, E., Nardy, A., Rosemberg, A., 1984. High- and low-TiO_2 flood basalts from the Paraná plateau (Brasil): Petrology and geochemical aspects bearing on their mantle origin. Neues Jahrb. Für Mineral. Abhandlungen 150 (January), 273–306.

Bellieni, G., Comin-Chiaramonti, P., Marques, L.S., Martínez, L.A., Melfi, A.J., Nardy, A. J.R., Piccirillo, E.M., Stolfa, D., 1986. Continental flood basalt from the central-western regions of the Paraná plateau (Paraguay and Argentina): petrology and petrogenetic aspects. Neues Jahrbuch.

Bellieni, G., Piccirillo, E.M., Cabazzini, G., Petrini, R., Comin-Chiaranmonti, P., Nardy, A.J.R., Civetta, L., Melfi, A.J., Zantedeschi, P., 1990. Low- and High-TiO_2 Mesozoic tholeiitic magmatism of the Maranhão Basin (NE-Brazil): K/Ar age, geochemistry, petrology, isotope characteristics and relationships with Mesozoic Low- and High-TiO_2 flood basalts of the Paraná basin (SE-Brazil). Neues Jahrb. Mineral. Abhandlungen 162 (1), 1–33.

Bellieni, G., Macedo, M.H.F., Petrini, R., Piccirillo, E.M., Cavazzini, G., Comin-Chiaramonti, P., Ernesto, M., Macedo, J.W.P., Martins, G., Melfi, A.J., Pacca, I.G., De Min, A., 1992. Evidence of magmatic activity related to Middle Jurassic and Early Cretaceous rifting from Northeastern Brazil (Ceará-Mirim): K/Ar age, palaeomagnetism, petrology and Sr-Nd isotope characteristics. Chem. Geol. 97, 9–32.

Benkhelil, J., Dainelli, P., Ponsard, J.F., Popoff, M., Saugy, L., 1988. Chapter 32 - The Benue trough: Wrench-fault related basin on the border of the equatorial Atlantic. In: Manspeizer, W. (Ed.), Triassic-Jurassic Rifting Continental Breakup and the Origin of the Atlantic Ocean and Passive Margins. Developments in Geotectonics, Vol. 22, 787–819. https://doi.org/10.1016/B978-0-444-42903-2.50037-3.

Bryan, S.E., Ernst, R.E., 2008. Revised definition of Large Igneous Provinces (LIPs). Earth-Sci. Rev. 86, 175–202. https://doi.org/10.1016/j.earscirev.2007.08.008.

Bryan, S.E., Ferrari, L., 2013. Large igneous provinces and silicic large igneous provinces: Progress in our understanding over the last 25 years. Bull. Geol. Soc. Am. 125, 1053–1078. https://doi.org/10.1130/B30820.1.

Carvas, K.Z., Vasconcelos, P.M.P., Marques, L.S., Ubide, T., Carmo, I.O., Babinski, M., 2021. Geochronology of mafic magmatism and hydrothermal alteration during early stages of South Atlantic opening. Geochim. Cosmochim. Acta 314, 358–380. https://doi.org/10.1016/j.gca.2021.08.017.

Carvas, K.Z., 2016. Diques mesozoicos subalcalinos de baixo titânio da Região dos Lagos (RJ): geoquímica e geocronologia ^{40}Ar/^{39}Ar. MSc thesis. Universidade de São Paulo, Instituto de Astronomia, Geofísica e Ciências Atmosféricas, São Paulo, Brazil, 112 p (in Portuguese).

Chaves, A.O., 2013. Enxames De Diques Máficos De Minas Gerais – O Estado Da Arte. Geonomos d, 29–33 (in Portuguese). https://doi.org/10.18285/geonomos.v21i1.253.

Chaves, A.O., 2014. Petrography and lithochemistry of the Early Cretaceous mafic dyke swarm Transminas (Minas Gerais, Brazil): geodynamic implications. Comun. Geol. 101, 163–167.

Christophersen, N., Hooper, R.P., 1992. Multivariate analysis of stream water chemical data' the use of principal components analysis for the end-member mixing problem. EM-space 28, 99–107.

Coelho, R.M., Chaves, A.O., 2017. Diques Máficos de Minas Gerais do Cretáceo Inferior: Idades Ar-Ar e correlação com a Província Ígnea Paraná-Etendeka. Geociências 36 (4), 613–622 (in Portuguese).

Coffin, M.F., Eldholm, O., 1994. Large Igneous Provinces: crustal structure, dimensions, and external consequences. Rev. Geophys. 32 (1), 1–36. https://doi.org/10.1029/93RG02508.

Coltice, N., Phillips, B.R., Bertrand, H., Ricard, Y., Rey, P., 2007. Global warming of the mantle at the origin of flood basalts over supercontinents. Geology 35, 391–394. https://doi.org/10.1130/G23240A.1.

Corval, A., 2009. Petrogênese e Contexto Geodinâmico das Suítes Basálticas Toleíticas (de alto-TiO_2 e baixo-TiO_2) do Cretáceo Inferior da Porção Centro-oriental do Enxame de Diques da Serra do Mar. Rio DE JanEiro. PhD ThEsis. UnivErsidaDE Estadual Do Rio DE JanEiro. CEntro DE TEcnologia E Ciências. FaculdaDE DE GEologia. 245 p (in Portuguese).

Corval, A., Valente, S.C., Duarte, B.P., Famelli, N., Zanon, M., 2008. Dados petrológicos dos diabásios dos setores centro-norte e nordeste do Enxame de Diques da Serra do Mar. Geochim. Bras. 22 (3), 159–177 (in Portuguese).

Coulon, C., Vidal, P., Dupuy, C., Baudin, P., Popoff, M., Maluski, H., Hermitte, D., 1996. The Mesozoic to early Cenozoic magmatism of the Benue Trough (Nigeria): geochemical evidence for the involvement of the St Helena Plume. J. Petrol. 37 (6), 1341–1358. https://doi.org/10.1093/petrology/37.6.1341.

Courtillot, V., Davaille, A., Besse, J., Stock, J., 2003. Three distinct types of hotspots in the Earth's mantle. Earth Planet. Sci. Lett. 205 (3–4), 295–308. https://doi.org/10.1016/S0012-821X(02)01048-8.

Cox, K.G., 1989. The role of mantle plumes in the development of continental drainage patterns. Nature 342, 873–877. https://doi.org/10.1038/342873a0.

Dantas, A.R., 2021. Caracterização geoquímica-isotópica e geocronologia do enxame de diques máficos Riacho do Cordeiro: extensão meridional da Província Magmática do Atlântico Equatorial. Msc thesis. Universidade de São Paulo, Instituto de Geociências São Paulo, Brazil. 74p (in Portuguese). https://doi.org/10.11606/D.44.2021.tde-02122021-093255.

Davies, D.L., Bouldin, D.W., 1979. A cluster separation measure. IEEE PAMI-1 (2), 224–227. https://doi.org/10.1109/tpami.1979.4766909.

de Carneiro, C., Fraser, S.J., Crósta, A.P., Silva, A.M., de Barros, C.E.M., 2012. Semiautomated geologic mapping using self-organizing maps and airborne geophysics in the Brazilian Amazon. Geophysics 77, K17–K24. https://doi.org/10.1190/geo2011-0302.1.

de Castro, D.L., Oliveira, D.C., Hollanda, M.H.B.M., 2018. Geostatistical interplay between geophysical and geochemical data: Mapping litho-structural assemblages of Mesozoic igneous activities in the Parnaíba Basin (NE Brazil). Surv. Geophys. 39 (4), 1–31. https://doi.org/10.1007/s10712-018-9463-5.

Janasi, V. de A., Negri, F. de A., Montanheiro, T.J., Freitas, V.A. de, Rocha, B.C., Reis, P. M., 2007. Geochemistry of the eocretacic basalt magmatism in the Piraju-Ourinhos region, SE Brazil, and implications to the stratigraphy of the Serra Geral Formation. Rev. Bras. Geociênc. 37(1), 148–162. https://doi.org/10.25249/0375-7536.2007371148162.

De Min, A., Callegaro, S., Marzoli, A., Nardy, A.J., Chiaradia, M., Marques, L.S., Gabbarrini, I., 2018. Insights into the petrogenesis of low- and high-Ti basalts: Stratigraphy and geochemistry of four lava sequences from the central Paraná basin. J. Volcanol. Geotherm. Res. 355, 232–252. https://doi.org/10.1016/j.jvolgeores.2017.08.009.

De Min, A., Piccirillo, E.M., Marzoli, A., Bellieni, G., Renne, P.R., Ernesto, M., Marques, L., 2003. The Central Atlantic Magmatic Province (CAMP) in Brazil: petrology, geochemistry, $^{40}Ar/^{39}Ar$ ages, paleomagnetism and geodynamic implications. In: Hames, W.E., Mchome, J.G., Renne, P.R., Ruppel, C. (Eds.). The Central Atlantic Magmatic Province: insights from fragments of Pangea. Geophys. Monogr. Ser. 136, 209–226. https://doi.org/10.1029/136GM06.

Deckart, K., Feraud, G., Marques, L.S., Bertrand, H., 1998. New time constraints on dyke swarms related to the Parana-Etendeka magmatic province, and subsequent South Atlantic opening, Southeastern Brazil. J. Volcanol. Geotherm. Res. 80, 67–83. https://doi.org/10.1016/S0377-0273(97)00038-3.

Erlank, A.J., Marsh, J.S., Duncan, A.R., Miller, R.M., Hawkesworth, C.J., Betton, P.J., Rex, D.C., 1984. Geochemistry and petrogenesis of the Etendeka volcanic rocks from SWA/Namibia. Geol. Soc. S. Afr. Spec. Publ. 13, 195–245.

Ernesto, M., Bellieni, G., Piccirillo, E.M., Marques, L.S., de Min, A., Pacca, I.G., Martins, G., Macedo, J.W.P., 2003. Paleomagnetic and geochemical constraints on the timing and duration of the CAMP activity in northeastern Brazil. Geophys. Monogr. Ser. 136, 129–149. https://doi.org/10.1029/136GM07.

Ernst, R.E., 2014. LIPs, rifting, and the supercontinentcycle. In: Ernst, R.E. (Ed.), Large Igneous Provinces. Cambridge University Press, Cambridge, pp. 339–369. https://doi.org/10.1017/cbo9781139025300.011.

Ernst, R.E., Buchan, K.L., 1997. Giant radiating dyke swarms: Their use in identifying pre-Mesozoic Large Igneous Provinces and mantle plumes. Geophys. Monogr. Ser. 100, 297–333. https://doi.org/10.1029/GM100p0297.

Ernst, R.E., Buchan, K.L., Campbell, I.H., 2005. Frontiers in Large Igneous Province research. Lithos 79 (3–4), 271–297. https://doi.org/10.1016/j.lithos.2004.09.004.

Ernst, R.E., Bond, D.P.G., Zhang, S., Buchan, K.L., Grasby, S.E., Youbi, N., El Bilali, H., Bekker, A., Doucet, L.S., 2021. Chapter 1 – large igneous province record through time and implications for secular environmental changes and geological time-scale boundaries. In: Ernst, R.E., Dickson, A.J., Bekker, A. (Eds.), LArge Igneous Provinces: A Driver of GlobAl EnvironmentAl and Biotic ChAnges. American Geophysical Union, pp. 1–26. https://doi.org/10.1002/9781119507444.ch1.

Ewart, A., Milner, S.C., Armstrong, R.A., Dungan, A.R., 1998. Etendeka Volcanism of the Goboboseb Mountains and Messum Igneous Complex, Namibia. Part I: Geochemical Evidence of Early Cretaceous Tristan Plume Melts and the Role of Crustal Contamination in the Parana-Etendeka CFB. J. Petrol. 39, 191–225. https://doi.org/10.1093/petrology/39.2.191.

Ewart, A., Marsh, J.S., Milner, S.C., Duncan, A.R., Kamber, B.S., Armstrong, R.A., 2004a. Petrology and geochemistry of early cretaceous bimodal continental flood volcanism of the NW Etendeka, Namibia. part 1: Introduction, mafic lavas and re-evaluation of mantle source components. J. Petrol. 45 (1), 59–105. https://doi.org/10.1093/petrology/egg083.

Ewart, A., Marsh, J.S., Milner, S.C., Duncan, A.R., Kamber, B.S., Armstrong, R.A., 2004b. Petrology and geochemistry of early cretaceous bimodal continental flood volcanism of the NW Etendeka, Namibia. part 2: Characteristics and petrogenesis of the high-Ti Latite and high-Ti and low-Ti voluminous quartz Latite Eruptives. J. Petrol. 45, 107–138. https://doi.org/10.1093/petrology/egg082.

Fernandes, L.B.M., Jardim de Sá, E.F., Vasconcelos, P.M.P., Córdoba, V.C., 2020. Structural controls and $^{40}Ar/^{39}Ar$ geochronological data of basic dike swarms in the eastern domain of the Parnaíba Basin, northeast Brazil. J. S. Am. Earth. Sci. 101,. https://doi.org/10.1016/j.jsames.2020.102601 102601.

Fernandez, O., Olaiz, A., Cascone, L., Hernandez, P., de Pereira, A., Tritlla, J., Ingles, M., Aida, B., Pinto, I., Rocca, R., Sanders, C., Herrá, A., Tur, N., 2020. Geophysical evidence for breakup volcanism in the Angola and Gabon passive margins. Mar. Pet. Geol. 116,. https://doi.org/10.1016/j.marpetgTristan-Gough hotspoteo.2020.104330 104330.

Florisbal, L.M., Heaman, L.M., de Assis Janasi, V., Bitencourt, M.F., 2014. Tectonic significance of the Florianópolis Dyke Swarm, Paraná-Etendeka Magmatic Province: A reappraisal based on precise U-Pb dating. J. Volcanol. Geotherm. Res. 289, 140–150. https://doi.org/10.1016/j.jvolgeores.2014.11.007.

Florisbal, L.M., Janasi, V.A., Bitencourt, M.F., Nardi, L.V.S., Marteleto, N.S., 2018. Geological, geochemical and isotope diversity of ~ 134 Ma dykes from the Florianópolis Dyke Swarm, Paraná Magmatic Province: Geodynamic controls on petrogenesis. J. Volcanol. Geotherm. Res. 355, 181–203. https://doi.org/10.1016/j.jvolgeores.2017.08.002.

Fodor, R.V., Sial, A.N., Mukasa, S.B., McKee, E.H., 1990. Petrology, isotope characteristics, and K-Ar ages of the Maranhão, northern Brazil, Mesozoic basalt province. Contrib. Mineral. Petrol. 104 (5), 555–567. https://doi.org/10.1007/BF00306664.

Foulger, G.R., 2018. Origin of the South Atlantic igneous province. J. Volcanol. Geotherm. Res. 355, 2–20. https://doi.org/10.1016/j.jvolgeores.2017.09.004.

Fraser, S.J., Dickson, B.L., 2007. A new method for data integration and integrated data interpretation: self-organizing maps. Proceedings of Exploration 07: Fifth Decennial International Conference on Mineral Exploration, 7, 907–910.

Friedel, M.J., 2011. Modeling hydrologic and geomorphic hazards across post-fire landscapes using a self-organizing map approach. Environ. Model. Softw. 26 (12), 1660–1674. https://doi.org/10.1016/j.envsoft.2011.07.001.

García, H.L., González, I.M., 2004. Self-organizing map and clustering for wastewater treatment monitoring. Eng. Appl. Artif. Intell. 17 (3), 215–225. https://doi.org/10.1016/j.engappai.2004.03.004.

Gibson, S.A., Thompson, R.N., Day, J.A., Humphris, S.E., Dickin, A.P., 2005. Melt-generation processes associated with the Tristan mantle plume: constraints on the origin of EM-1. Earth Planet. Sci. Lett. 237 (3–4), 744–767. https://doi.org/10.1016/j.epsl.2005.06.015.

Gladczenko, T.P., Hinz, K., Eldholm, O., Meyer, H., Neben, S., Skogseid, J., 1997. South Atlantic volcanic margins. J. Geol. Soc. London. 154, 465–470. https://doi.org/10.1144/gsjgs.154.3.0465.

Gomes, A.S., Vasconcelos, P.M., 2021. Geochronology of the Paraná-Etendeka large igneous province. Earth-Sci. Rev. 220,. https://doi.org/10.1016/j.earscirev.2021.103716 103716.

Greenough, J.D., McDivitt, J.A., 2018. Earth's evolving subcontinental lithospheric mantle: inferences from LIP continental flood basalt geochemistry. Int. J. Earth Sci. 107 (3), 787–810. https://doi.org/10.1007/s00531-017-1493-6.

Guedes, E., Heilbron, M., Vasconcelos, P.M., de Morisson Valeriano, C., Horta de Almeida, J.C., Teixeira, W., Filho, A.T., 2005. K-Ar and $^{40}Ar/^{39}Ar$ ages of dikes emplaced in the onshore basement of the Santos Basin, Resende area, SE Brazil: Implications for the south Atlantic opening and Tertiary reactivation. J. South Am. Earth Sci. 18, 371–382. https://doi.org/10.1016/j.jsames.2004.11.008.

Guedes, E., Heilbron, M., de Morisson Valeriano, C., de Almeida, J.C.H., Szatmari, P., 2016. Evidence of Gondwana early rifting process recorded by Resende-Ilha Grande Dike Swarm, southern Rio de Janeiro. Brazil. J. S. Am. Earth Sci. 67, 11–24. https://doi.org/10.1016/j.jsames.2016.01.004.

Guiraud, R., Maurin, J.C., 1992. Early Cretaceous rifts of Western and Central Africa: an overview. Tectonophysics 213 (1–2), 153–168. https://doi.org/10.1016/0040-1951(92)90256-6.

Hart, S.R., 1984. The DUPAL anomaly: a large-scale isotopic anomaly in the southern hemisphere. Nature 309, 753–756.

Hartmann, L.A., Arena, K.R., Duarte, S.K., 2012. Geological relationships of basalts, andesites and sand injectites at the base of the Paraná volcanic province, Torres, Brazil. J. Volcanol. Geotherm. Res. 237–238, 97–111. https://doi.org/10.1016/j.jvolgeores.2012.05.017.

Hartmann, L.A., Arena, K.R., Duarte, S.K., Pertille, J., 2013. Long-distance lava correlation in the Paraná volcanic province along the Serra Geral cuesta, southeastern Brazil. Int. J. Earth Sci. 102, 1655–1669. https://doi.org/10.1007/s00531-013-0899-z.

Hartmann, L.A., Baggio, S.B., Brückmann, M.P., Knijnik, D.B., Lana, C., Massonne, H.J., Opitz, J., Pinto, V.M., Sato, K., Tassinari, C.C.G., Arena, K.R., 2019. U-Pb geochronology of Paraná volcanics combined with trace element geochemistry of the zircon crystals and zircon Hf isotope data. J. South Am. Earth Sci. 89, 219–226. https://doi.org/10.1016/j.jsames.2018.11.026.

Hawkesworth, C., Mantovani, M., Peate, D., 1988. Lithosphere remobilization during Paraná CFB magmatism. J. Petrol. Special_Vol. 205–223. https://doi.org/10.1093/petrology/Special_Volume.1.205.

Heilbron, M., Guedes, E., Mane, M., Valeriano, C.M., Tupinambá, M., Almeida, J., Silva, L.G.E., Duarte, B.P., Dela Favera, J.C., Viana, A., 2018. Geochemical and temporal provinciality of the magmatism of the eastern Parnaíba Basin, NE Brazil. In: Daly, M.C., Fuck, R.A., Julià, J., Macdonald, D.I.M., Watts, A.B. (Eds.), Cratonic basin formation: a case study of the Parnaíba Basin of Brazil. Geol. Soc. Spec. Publ., London, 472. https://doi.org/10.1144/SP472.11.

Heit, B., Yuan, X., Weber, M., Geissler, W., Jokat, W., Lushetile, B., Hoffmann, K., 2015. Crustal thickness and Vp/Vs ratio in NW Namibia from receiver functions: Evidence for magmatic underplating due to mantle plume-crust interaction. Geophys. Res. Lett. 42 (9), 3330–3337. https://doi.org/10.1002/2015GL063704.

Hodgkinson, J.H., Fraser, S.J., Donchak, P., 2013. Using self-organising maps to derive lithological boundaries from geophysically-derived data in the Mt. Isa region, Queensland. ASEG Extended Abstracts 2012 (1), 1–4. https://doi.org/10.1071/aseg2012ab359.

Hoernle, K., Rohde, J., Hauff, F., Garbe-Schönberg, D., Homrighausen, S., Werner, R., Morgan, J.P., 2015. How and when plume zonation appeared during the 132 Myr evolution of the Tristan Hotspot. Nat. Commun. 6. https://doi.org/10.1038/ncomms8799.

Hollanda, M.H.B.M., Martins Pimentel, M., Jardim de Sá, E.F., 2003. Paleoproterozoic subduction-related metasomatic signatures in the lithospheric mantle beneath NE Brazil: Inferences from trace element and Sr-Nd-Pb isotopic compositions of Neoproterozoichigh-K igneous rocks. J. South Am. Earth Sci. 15, 885–900. https://doi.org/10.1016/S0895-9811(03)00014-2.

Hollanda, M.H.B.M., Pimentel, M.M., Oliveira, D.C., de Sá, E.F.J., 2006. Lithosphere-asthenosphere interaction and the origin of Cretaceous tholeiitic magmatism in Northeastern Brazil: Sr-Nd-Pb isotopic evidence. Lithos 86, 34–49. https://doi.org/10.1016/j.lithos.2005.04.004.

Hollanda, M.H.B.M., Archanjo, C.J., Macedo Filho, A.A., Fossen, H., Ernst, R.E., de Castro, D.L., Melo, A.C.C., Oliveira, A.L., 2019. The Mesozoic Equatorial Atlantic Magmatic Province (EQUAMP). In: Srivastava, R.K., Ernst, R.E., Peng, P. (Eds.), Dyke SwArms of the World: A Modern Perspective. Springer, Singapore, pp. 87–110. https://doi.org/10.1007/978-981-13-1666-1.

Homrighausen, S., Hoernle, K., Hauff, F., Wartho, J.A., van den Bogaard, P., Garbe-Schönberg, D., 2019. New age and geochemical data from the Walvis Ridge: The temporal and spatial diversity of South Atlantic intraplate volcanism and its possible origin. Geochim. Cosmochim. Acta 245, 16–34. https://doi.org/10.1016/j.gca.2018.09.002.

Hosseini, K., Matthews, K.J., Sigloch, K., Shephard, G.E., Domeier, M., Tsekhmistrenko, M., 2018. SubMachine: Web-Based tools for exploring seismic tomography and other models of Earth's deep interior. Geochem. Geophys. 19. https://doi.org/10.1029/2018GC007431.

Keiding, J.K., Trumbull, R.B., Veksler, I.V., Jerram, D.A., 2011. On the significance of ultra-magnesian olivines in basaltic rocks. Geology 39 (12), 1095–1098. https://doi.org/10.1130/G32214.1.

Janasi, V.A., Freitas, V.A., Heaman, L.H., 2011. The onset of flood basalt volcanism, Northern Paraná Basin, Brazil: A precise U-Pb baddeleyite/zircon age for a Chapecó-type dacite. Earth Planet. Sci. Lett. 302 (1–2), 147–153. https://doi.org/10.1016/j.epsl.2010.12.005.

Keiding, J.K., Frei, O., Renno, A.D., Veksler, I.V., Trumbull, R.B., 2013. Conditions of magma crystallization in the Henties Bay-Outjo dyke swarm, Namibia: implications for the feeder system of continental flood basalts. Lithos 179, 16–27. https://doi.org/10.1016/j.lithos.2013.07.018.

King, S.D., Anderson, D.L., 1995. An alternative mechanism of flood basalt formation. Earth Planet. Sci. Lett. 136, 269–279. https://doi.org/10.1016/0012-821X(95)00205-Q.

Kirstein, L.A., Kelley, S., Hawkesworth, C., Turner, S., Mantovani, M., Wijbrans, J., 2001. Protracted felsic magmatic activity associated with the opening of the South Atlantic. J. Geol. Soc. London 158, 583–592. https://doi.org/10.1144/jgs.158.4.58.

Klein, E.L., Angélica, R.S., Harris, C., Jourdan, F., Babinski, M., 2013. Mafic dykes intrusive into Pre-Cambrian Rocks of the São Luís Cratonic Fragment and Gurupi Belt (Parnaíba Province), North-northeastern Brazil: Geochemistry, Sr-Nd-Pb-O isotopes, $^{40}Ar/^{39}Ar$ geochronology, and relationships to CAMP magmatism. Lithos 172–173, 222–242. https://doi.org/10.1016/j.lithos.2013.04.015.

Kohonen, T., 1982. Self-organized formation of topologically correct feature maps. Biol. Cybern. 43 (1), 59–69. https://doi.org/10.1007/BF00337288.

Kohonen, T., 2001. Self-Organizing Maps. Springer-Verlag, Berlin, Heidelberg, New York.

Kohonen, T., 2013. Essentials of the self-organizing map. Neural Networks 37, 52–65. https://doi.org/10.1016/j.neunet.2012.09.018.

Krob, F.C., Glasmacher, A.U., Bunge, H., Friedrich, A.M., Hackspacher, P.C., 2020. Application of stratigraphic frameworks and thermochronological data on the Mesozoic SW Gondwana intraplate environment to retrieve the Paraná-Etendeka plume movement. Gondwana Res. 84, 81–110.

Le Maitre, R.W., 2002. Igneous Rocks – A Classification and Glossary of Terms. Recommendations of the IUGS Subcommission on the Systematics of Igneous Rocks. Cambridge University Press, Cambridge.

Licht, O.A.B., 2018. A revised chemo-chrono-stratigraphic 4-D model for the extrusive rocks of the Paraná Igneous Province. J. Volc. Geoth. Res. 355, 32–54.

Löhr, S.C., Grigorescu, M., Hodgkinson, J.H., Cox, M.E., Fraser, S.J., 2010. Iron occurrence in soils and sediments of a coastal catchment. A multivariate approach using self organising maps. Geoderma 156 (3–4), 253–266. https://doi.org/10.1016/j.geoderma.2010.02.025.

Loule, J.P., Pospisil, L., 2013. Geophysical evidence of Cretaceous volcanics in Logone Birni Basin (Northern Cameroon), Central Africa, and consequences for the West and Central African Rift System. Tectonophysics 583, 88–100. https://doi.org/10.1016/j.tecto.2012.10.021.

Lu, C., Grand, S.P., Lai, H., Garnero, E.J., 2019. TX2019slab: A new P and S tomography model incorporating subducting slabs. J. Geophys. Res. Solid Earth. 124 (11), 11549–11567. https://doi.org/10.1029/2019jb017448.

Macêdo Filho, A.A., Archanjo, C.J., Hollanda, M.H.B.M., Negri, F.A., 2019. Mineral chemistry and crystal size distributions of mafic dikes and sills on the eastern border of the Parnaíba Basin, NE Brazil. J. Volcanol. Geotherm. Res. 377, 69–80. https://doi.org/10.1016/j.jvolgeores.2019.03.021.

Macêdo Filho, A.A., Hollanda, M.H.B.M., 2022. Petrogenesis of Mesozoic giant dike swarms and geodynamical insights about EMI-Gough flavors in the Equatorial Atlantic Magmatic Province. Lithos 412–413,. https://doi.org/10.1016/j.lithos.2022.106611 106611.

Macêdo Filho, A.A., 2021. Geochemical characterization of the Equatorial Atlantic Magmatic Province and its correlation with other magmatic events related to the South Atlantic Opening. PhD dissertation. Universidade de São Paulo, São Paulo, Brazil, 282p. https://doi.org/10.11606/T.44.2021.tde-18012022-115836.

Machado, F.B., Nardy, A.J.R., de Oliveira, M.A.F., 2007. Geologia e aspectos petrológicos das rochas intrusivas e efusivas mesozóicas de parte da borda leste da bacia do Paraná no estado de São Paulo in Portuguese Rev. Bras. Geociênc. 37 (1), 64–80. https://doi.org/10.25249/0375-7536.20073716480.

Machado, F.B., Rocha-Júnior, E.R.V., Marques, L.S., Nardy, A.J.R., 2015. Volcanological aspects of the northwest region of Paraná continental flood basalts (Brazil). J. Geophys. Res. Solid Earth 6, 227–241. https://doi.org/10.5194/se-6-227-2015.

Machado, F.B., Rocha-Júnior, E.R.V., Marques, L.S., Nardy, A.J.R., Zezzo, L.V., Marteleto, N.S., 2018. Geochemistry of the northern Paraná Continental Flood Basalt (PCFB) province: Implications for regional chemostratigraphy. Brazilian J. Geol. 48, 177–199. https://doi.org/10.1590/2317-4889201820180098.

Maluski, H., Coulon, C., Popoff, M., Baudin, P., 1995. $^{40}Ar/^{39}Ar$ chronology, petrology and geodynamic setting of Mesozoic to early Cenozoic magmatism from the Benue Trough. Nigeria. J. Geol. Soc. 152 (2), 311–326. https://doi.org/10.1144/gsjgs.152.2.0311.

Mantovani, M.S.M., Hawkesworth, C.J., 1990. An inversion approach to assimilation and fractional crystallisation processes. Contrib. To Mineral. Petrol. 105, 289–302. https://doi.org/10.1007/BF00306540.

Mantovani, M.S.M., Marques, L.S., De Sousa, M.A., Civetta, L., Atalla, L., Innocenti, F., 1985. Trace element and strontium isotope constraints on the origin and evolution of Paraná continental flood basalts of Santa Catarina state (Southern Brazil). J. Petrol. 26, 187–209. https://doi.org/10.1093/petrology/26.1.187.

Mantovani, S.M., Peate, D.W., Hawkesworth, C.J., 1988. Geochemical stratigraphy of Parana continental flood basalts: a contribution from boreholes samples. Mesozoic Flood Volcanism Parana Basin, 15–24.

Marques, L.S., Dupré, B., Piccirillo, E.M., 1999. Mantle source compositions of the Parana Magmatic Province (southern Brazil): evidence from trace element and Sr-Nd-Pb isotope geochemistry. J. Geodyn. 28, 439–458. https://doi.org/10.1016/S0264-3707(99)00020-4.

Marques, L.S., Rocha-Júnior, E.R.V., Babinski, M., Carvas, K.Z., Petronilho, L.A., De Min, A., 2016. Lead isotope constraints on the mantle sources involved in the genesis of Mesozoic high-Ti tholeiite dykes (Urubici type) from the São Francisco Craton (Southern Espinhaço, Brazil). Braz. J. Geol. 46, 105–122. https://doi.org/10.1590/2317-4889201620150010.

Marques, L.S., De Min, A., Rocha-Júnior, E.R.V., Babinski, M., Bellieni, G., Figueiredo, A.M.G., 2018. Elemental and Sr-Nd-Pb isotope geochemistry of the Florianópolis Dyke Swarm (Paraná Magmatic Province): crustal contamination and mantle source constraints. J. Volcanol. Geotherm. Res. 355, 149–164. https://doi.org/10.1016/j.jvolgeores.2017.07.005.

Marsh, J.S., Ewart, A., Milner, S.C., Duncan, A.R., Miller, R.M.G., 2001. The Etendeka Igneous Province: Magma types and their stratigraphic distribution with implications for the evolution of the Paraná-Etendeka flood basalt province. Bull. Volcanol. 62 (6–7), 464–486. https://doi.org/10.1007/s004450000115.

Marsh, J.S., Swart, R., 2018. The Bero Volcanic Complex: extension of the Paraná-Etendeka Igneous Province into SW Angola. J. Volcanol. Geotherm. Res. 355, 21–31. https://doi.org/10.1016/j.jvolgeores.2016.10.011.

Marzoli, A., Renne, P.R., Piccirillo, E.M., 2000. Ar/Ar geochronology of Mesozoic continental basaltic magmatism, and the opening of the central, equatorial and southern Atlantic Ocean. Penrose 2000, Volcanic Rifted Margins. University of London, p. 54.

Marzoli, A., Renne, P.R., Piccirillo, E.M., Ernesto, M., Bellieni, G., De Min, A., 1999a. Extensive 200–million–year old continental flood basalts of the Central Atlantic Magmatic Province. Science 284, 616–618. https://doi.org/10.1126/science.284.5414.616.

Marzoli, A., Melluso, L., Morra, V., Renne, P.R., Sgrosso, I., D'Antonio, M., Duarte Morais, L., Morais, E.A.A., Ricci, G., 1999b. Geochronology and petrology of Cretaceous basaltic magmatism in the Kwanza basin (western Angola), and relationships with the Parana-Etendeka continental flood basalt province. J. Geodyn. 28, 341–356. https://doi.org/10.1016/S0264-3707(99)00014-9.

Masquelin, H., Aïfa, T., Muzio, R., Hallot, E., Veroslavsky, G., Bonnevalle, L., 2009. The Cuaró Mesozoic doleritic dyke swarm, southern Paraná basin, Uruguay: Examples of superimposed magnetic fabrics? Comptes Rendus - Geosci. 341, 1003–1015. https://doi.org/10.1016/j.crte.2009.07.004.

Matos, R.D., 1992. The Northeast Brazilian Rift System. Tectonics 11 (4), 766–791. https://doi.org/10.4324/9780429496073-6.

Matos, R.M., 2000. Tectonic evolution of the equatorial South Atlantic the Brazilian and West African Equatorial Margins Comprise America. Atlantic Rifts and Continental Margins 331–354. https://doi.org/10.1029/GM115p0331.

Matthews, K.J., Maloney, K.T., Zahirovic, S., Williams, S.E., Seton, M., Müller, R.D., 2016. Global plate boundary evolution and kinematics since the late Paleozoic. Glob. Planet. Change 146, 226–250. https://doi.org/10.1016/j.gloplacha.2016.10.002.

McMaster, M., Almeida, J., Heilbron, M., Guedes, E., Mane, M.A., Linus, J.H., 2019. Characterisation and tectonic implications of the Early Cretaceous, Skeleton Coast Dyke Swarm. NW Namibia. J. Afr. Earth Sci. 150, 319–336. https://doi.org/10.1016/j.jafrearsci.2018.11.010.

Melo, A.C.C., de Castro, D.L., Bezerra, F.H.R., Bertotti, G., 2016. Rift fault geometry and evolution in the Cretaceous Potiguar Basin (NE Brazil) based on fault growth models. J. South Am. Earth Sci. 71, 96–107. https://doi.org/10.1016/j.jsames.2016.07.006.

Melo, A.C.C., de Castro, D.L., Fraser, S.J., de Macêdo Filho, A.A., 2021. Using self-organizing maps in airborne geophysical data for mapping mafic dyke swarms in NE Brazil. J. Appl. Geophys. 192,. https://doi.org/10.1016/j.jappgeo.2021.104377 104377.

Melo, A.C.C., de Castro, D., Oliveira, D.C., Hollanda, M.H.B.M., 2022. Mesozoic dike swarms in Borborema Province (NE Brazil): A structural analysis based on airborne geophysical data and field work. J. South Am. Earth Sci. 113,. https://doi.org/10.1016/j.jsames.2021.103650 103650.

Mercer, C.M., Hodges, K.V., 2016. ArAR — a software tool to promote the robust comparison of K – Ar and $^{40}Ar/^{39}Ar$ dates published using different decay, isotopic, and monitor-age parameters. Chem. Geol. 440, 148–163. https://doi.org/10.1016/j.chemgeo.2016.06.020.

Merle, R., Marzoli, A., Bertrand, H., Reisberg, L., Verati, C., Zimmermann, C., Chiaradia, M., Belienni, G., Ernesto, M., 2011. $^{40}Ar/^{39}Ar$ ages and Sr–Nd–Pb–Os geochemistry of CAMP tholeiites from western Maranhão Basin (NE Brazil). Lithos 122, 137–151. https://doi.org/10.1016/j.lithos.2010.12.010.

Miyashiro, A., 1978. Nature of alkalic volcanic rock series. Contrib. Mineral. Petrol. 66 (1), 91–104. https://doi.org/10.1007/BF00376089.

Mizusaki, A.M.P., Saracchini, F.E., 1991. Catálogo geral de dados geocronológicos da Petrobras. Internal Report, p. 24.

Müller, R.D., Zahirovic, S., Williams, S.E., Cannon, J., Seton, M., Bower, D.J., Tetley, M. G., Heine, C., Le Breton, E., Liu, S., Russell, S.H.J., Yang, T., Leonard, J., Gurnis, M., 2019. A global plate model including lithospheric deformation along major rifts and orogens since the Triassic. Tectonics 38 (6), 1884–1907. https://doi.org/10.1029/2018TC005462.

Muzio, R., Scaglia, F., Masquelin, H., 2012. Petrochemistry of Mesozoic mafic intrusions related to the Paraná magmatic province, Uruguay. Int. Geol. Rev. 54, 844–860. https://doi.org/10.1080/00206814.2011.588487.

Muzio, R., Peel, E., Porta, N., Scaglia, F., 2017. Mesozoic dykes and sills from Uruguay: Sr – Nd isotope and trace element geochemistry. J. South Am. Earth Sci. 77, 92–107. https://doi.org/10.1016/j.jsames.2017.04.016.

Nardy, A.J.R., Rosa, M.C., Luchetti, A.C.F., Ferreira, M.L.C., Machado, F.B., 2011. Parâmetros físicos pré-eruptivos do magmatismo ácido da província magmática do Paraná: Resultados preliminares. Geociências 30 (4), 575–588.

Ngonge, E.D., Archanjo, C.J., Hollanda, M.H.B.M., 2013. Plagioclase crystal size distribution in some tholeiitic mafic dikes in Cabo Frio-Búzios, Rui de Janeiro. Brazil. J. Volcanol. Geotherm. Res. 255, 26–42. https://doi.org/10.1016/j.jvolgeores.2013.01.009.

Ngonge, E.D., de Hollanda, M.H.B.M., Archanjo, C.J., de Oliveira, D.C., Vasconcelos, P. M.P., Muñoz, P.R.M., 2016. Petrology of continental tholeiitic magmas forming a 350-km-long Mesozoic dyke swarm in NE Brazil: Constraints of geochemical and isotopic data. Lithos 258–259, 228–252. https://doi.org/10.1016/j.lithos.2016.04.008.

Oliveira, D.C., 1992. O papel do Enxame de Diques Rio Ceará Mirim na evolução tectônica do nordeste oriental (Brasil): implicações na formação do Rifte Potiguar. Universidade Federal de Ouro Preto, Ouro Preto, Brazil. MSc thesis.

Oliveira, A.L., Pimentel, M.M., Fuck, R.A., Oliveira, D.C., 2018. Petrology of Jurassic and Cretaceous basaltic formations from the Parnaíba Basin, NE Brazil: correlations and associations with large igneous provinces. In: Daly, M.C., Fuck, R.A., Julià, J., Macdonald, D.I.M., Watts, A.B. (Eds.), Cratonic basin formation: a case study of the Parnaíba Basin of Brazil. Geol. Soc. Spec. Publ. London 472 (1), SP472.20. https://doi.org/10.1144/SP472.9.

Oliveira, A.L., Hollanda, M.H.B.M., Siqueira, R., Macêdo Filho, A.A., 2021. Using a 'speedy' unspiked K-Ar methodology to investigate age patterns in giant mafic dyke swarms. Geol. Soc. Spec. Publ., London 518 (1), 285. https://doi.org/10.1144/SP518-2020-250.

Owen-Smith, T.M., Trumbull, R.B., Bauer, K., Keiding, J.K., Will, T.M., 2021. A neural network application to assess magma diversity in the Etendeka igneous province. Namibia. S. Afr. J. Geol. 124 (2), 481–498. https://doi.org/10.25131/sajg.124.0034.

Pearce, J.A., Ernst, R.E., Peate, D.W., Rogers, C., 2021. LIP printing: Use of immobile element proxies to characterize Large Igneous Provinces in the geologic record. Lithos 392–393,. https://doi.org/10.1016/j.lithos.2021.106068 106068.

Peate, D.W., 1997. The Paraná-Etendeka province. Geophys. Monogr. Ser. 100, 217–245. https://doi.org/10.1029/GM100p0217.

Peate, D.W., Hawkesworth, C.J., 1996. Lithospheric to asthenospheric transition in low-Ti flood basalts from southern Paraná. Brazil. Chem. Geol. 127, 1–24. https://doi.org/10.1016/0009-2541(95)00086-0.

Peate, D.W., Hawkesworth, C.J., Mantovani, M.S.M., 1992. Chemical stratigraphy of the Paraná lavas (South America): classification of magma types and their spatial distribution. Bull. Volcanol. 55 (1–2), 119–139. https://doi.org/10.1007/BF00301125.

Peate, D.W., Hawkesworth, C.J., Mantovani, M.M.S., Rogers, N.W., Turner, S.P., 1999. Petrogenesis and stratigraphy of the high-Ti/Y Urubici magma type in the Parana Flood Basalt Province and implications for the nature of 'Dupal'-type mantle in the South Atlantic Region. J. Petrol. 40 (3), 451–473. https://doi.org/10.1093/petroj/40.3.451.

Penn, B.S., 2005. Using self-organizing maps to visualize high-dimensional data. Comput. Geosci. 31, 531–544. https://doi.org/10.1016/j.cageo.2004.10.009.

Pessano, P.C., Ganade, C.E., Tupinambá, M., Teixeira, W., 2021. Updated map of the mafic dike swarms of Brazil based on airborne geophysical data. J. South Am. Earth Sci. 107,. https://doi.org/10.1016/j.jsames.2020.103076 103076.

Petersohn, E., Gouvea, E.M., 2009. Geologia e geoquímica da soleira de Reserva, estado do Paraná. Rev. Bras. Geociênc. 39 (4), 740–750. https://doi.org/10.25249/0375-7536.2009394740750.

Petrini, R., Civetta, L., Piccirillo, E.M., Bellieni, G., Comin-chiaramonti, P., Marques, L. S., Melfi, A.J., 1987. Mantle heterogeneity and crustal contamination in the genesis of low-Ti continental flood basalts from the Paranà plateau (Brazil): Sr-Nd isotope and geochemical evidence. J. Petrol. 28, 701–726. https://doi.org/10.1093/petrology/28.4.701.

Piccirillo, E.M., Bellieni, G., Cavazzini, G., Comin-Chiaramonti, P., Petrini, R., Melfi, A. J., Pinese, J.P.P., Zantadeschi, P., De Min, A., 1990. Early Cretaceous tholeiitic dyke swarms from the Ponta Grossa Arch (southeast Brazil): Petrology, Sr-Nd isotopes and genetic relationships with the Paraná flood volcanics. Chem. Geol. 89, 19–48. https://doi.org/10.1016/0009-2541(90)90058-F.

Piccirillo, E.M., Melfi, A.J., Comin-Chiaramonti, P., Bellieni, G., Ernesto, M., Marques, L.S., Nardy, A.J.R., Pacca, I.G., Roisenberg, A., Stolfa, D., 1988. Continental flood volcanism from the Parana basin (Brazil). In: Macdougall, J.D. (Ed.), Continental Flood Basalts. Petrology and Structural Geology, vol. 3. Springer, Dordrecht. https://doi.org/10.1007/978-94-015-7805-9_6.

Pinto, V.M., Hartmann, L.A., Santos, J.O.S., McNaughton, N.J., Wildner, W., 2011. Zircon U-Pb geochronology from the Paraná bimodal volcanic province support a brief eruptive cycle at ~135 Ma. Chem. Geol. 281, 93–102. https://doi.org/10.1016/j.chemgeo.2010.11.031.

Rämö, O.T., Heikkilä, P.A., Pulkkinen, A.H., 2016. Geochemistry of Paraná-Etendeka basalts from Misiones, Argentina: Some new insights into the petrogenesis of high-Ti continental flood basalts. J. South Am. Earth Sci. 67, 25–39. https://doi.org/10.1016/j.jsames.2016.01.008.

Raposo, M.I.B., Ernesto, M., Renne, P.R., 1998. Paleomagnetism and $^{40}Ar/^{39}Sr$ dating of the early Cretaceous Florianopolis dike swarm (Santa Catarina Island), Southern Brazil. Phys. Earth Planet. Inter. 108, 275–290. https://doi.org/10.1016/S0031-9201(98)00102-2.

Reid, D.L., Rex, D.C., 1994. Cretaceous dykes associated with the opening of the South Atlantic: the Mehlberg dyke, northern Richtersveld. South African J. Geol. 97, 135–145.

Renne, P.R., Deckart, K., Ernesto, M., Féraud, G., Piccirillo, E.M., 1996a. Age of the Ponta Grossa dike swarm (Brazil), and implications to Paraná flood volcanism. Earth Planet. Sci. Lett. 144, 199–211. https://doi.org/10.1016/0012-821x(96)00155-0.

Renne, P.R., Glen, J.M., Milner, S.C., Duncan, A.R., 1996b. Age of Etendeka flood volcanism and associated intrusions in southwestern Africa. Geology 24, 659–662. https://doi.org/10.1130/0091-7613(1996)024<0659:AOEFVA>2.3.CO;2.

Renne, P.R., Balco, G., Ludwig, K.R., Mundil, R., Min, K., 2011. Response to the comment by W. H. Schwarz et al. on "Joint determination of ^{40}K decay constants and $^{40}Ar^*$ / ^{40}K for the Fish Canyon sanidine standard, and improved accuracy for $^{40}Ar/^{39}Ar$ geochronology". Geochim. Cosmochim. Acta 75 (17), 5097–5100. https://doi.org/10.1016/j.gca.2011.06.021.

Renner, L.C., 2010. Geoquímica de Sills basálticos da Formação Serra Geral, Sul do Brasil, com base em rocha total e micro-análise de minerais. Universidade Federal do Rio Grande do Sul, Instituto de Geociências, Porto Alegre, Brazil, p. 226.

Richards, P.C., Stone, P., Kimbell, G.S., McIntosh, W.C., Phillips, E.R., 2013. Mesozoic magmatism in the Falkland Islands (South Atlantic) and their offshore sedimentary basins. J. Pet. Geol. 36, 61–73. https://doi.org/10.1111/jpg.12542.

Rocha, B.C., Janasi, V.A., Polo, L.A., Rocha, B.C., Davies, J.H.F.L., Schaltegger, U., Greber, N.D., Davies, J.H.F.L., Nardy, A.J.R., Lucchetti, A.C.F., Greber, N.D., 2020. Rapid eruption of silicic magmas from the Paraná magmatic province (Brazil) did not trigger the Valanginian event. Geology 48, 1174–1178. https://doi.org/10.1130/G47766.1.

Rocha-Júnior, E.R.V., Puchtel, I.S., Marques, L.S., Walker, R.J., Machado, F.B., Nardy, A. J.R., Babinski, M., Figueiredo, A.M.G., 2012. Re-Os isotope and highly siderophile element systematics of the Paraná continental flood basalts (Brazil). Earth Planet. Sci. Lett. 337–338, 164–173. https://doi.org/10.1016/j.epsl.2012.04.050.

Rocha-Júnior, E.R.V., Marques, L.S., Babinski, M., Nardy, A.J.R., Figueiredo, A.M.G., Machado, F.B., 2013. Sr-Nd-Pb isotopic constraints on the nature of the mantle sources involved in the genesis of the high-Ti tholeiites from northern Paraná Continental Flood Basalts (Brazil). J. South Am. Earth Sci. 46, 9–25. https://doi.org/10.1016/j.jsames.2013.04.004.

Rocha-Júnior, E.R.V., Marques, L.S., Babinski, M., Machado, F.B., Petronilho, L.A., Nardy, A.J.R., 2020. A telltale signature of Archean lithospheric mantle in the Paraná continental flood basalts genesis. Lithos 364–365,. https://doi.org/10.1016/j.lithos.2020.105519 105519.

Rodrigues, I.S., Vasconcelos, C.S., Carmo, I.O., Costa, J., Morales, I.V.F., Morais Neto, J. M., Simbras, F.M., Vasconcelos, P.M.P., 2016. Basalto Santiago do Norte – nova ocorrência de rocha ígnea na Bacia Parecis-Alto Xingu, MT. Anais Do 48° Congresso Brasileiro De Geologia.

Rohde, J., Hoernle, K., Hauff, F., Werner, R., O'Connor, J., Class, C., Garbe-Schönberg, D., Jokat, W., 2013. 70 Ma chemical zonation of the Tristan-Gough hotspot track. Geology 41, 335–338. https://doi.org/10.1130/G33790.1.

Rosset, A., De Min, A., Marques, L.S., Macambira, M.J.B., Ernesto, M., Renne, P.R., Piccirillo, E.M., 2007. Genesis and geodynamic significance of Mesoproterozoic and Early Cretaceous tholeiitic dyke swarms from the São Francisco craton (Brazil). J. South Am. Earth Sci. 24 (1), 69–92. https://doi.org/10.1016/j.jsames.2007.02.002.

Rubert, R.R., Mizusaki, A.M.P., Martinelli, A.G., 2019. Mesozoic tectonic in the deposition and evolution of Cretaceous sedimentary packages of the Parecis Basin, center-western Brazil. J. South Am. Earth Sci. 93, 140–154. https://doi.org/10.1016/j.jsames.2019.05.002.

Ryberg, T., Haberland, C., Haberlau, T., Weber, M.H., Bauer, K., Behrmann, J.H., Jokat, W., 2015. Crustal structure of northwest Namibia: Evidence for plume-rift-continent interaction 43, 739–742. https://doi.org/10.1130/G36768.1.

Santiago, R., de Andrade Caxito, F., Aparecida Neves, M., Luiz Dantas, E., de Medeiros, B., Júnior, E., Nascimento Queiroga, G., 2020. Two generations of mafic dyke swarms in the southeastern Brazilian coast: reactivation of structural lineaments during the gravitational collapse of the Araçuaí-Ribeira Orogen (500 Ma) and West Gondwana breakup (140 Ma). Precambrian Res. 340,. https://doi.org/10.1016/j.precamres.2019.105344 105344.

Santos, T.D., 2006. Petrogênese dos basaltos de baixo-TiO_2 do Enxame de Diques da Serra do Mar na Região dos Lagos, RJ. In: MSc Thesis. UniversidaDe Do EstaDo Do Rio De Janeiro. Rio De Janeiro, p. 139.

Sarmento, C.C.T., Sommer, C.A., De Lima, E.F., De Oliveira, D.S., 2014. Corpos hipabissais correlacionados à Formação Serra Geral na região do Cerro do Coronel, RS: Geologia e petrologia. Geologia USP - Serie Cientifica 14 (2), 23–44. https://doi.org/10.5327/Z1519-874X201400020002.

Sarmento, C.C.T., Sommer, C.A., Lima, E.F., 2017. Mafic subvolcanic intrusions and their petrologic relation with the volcanism in the south hinge Torres Syncline, Paraná-Etendeka Igneous Province, southern Brazil. J. South Am. Earth Sci. 77, 70–91. https://doi.org/10.1016/j.jsames.2017.04.017.

Sarmento, C.C.T., Sommer, C.A., de Lima, E.F., Barreto, C.J.S., de Magalhães May Rossetti, L., Lafon, J.M., 2020. Mafic subvolcanic intrusions from the southern Paraná-Etendeka Large Igneous Province, Brazil: Insights from geochemistry and Sr–Nd–Pb isotopes. Geol. J. 56, 1143–1166. https://doi.org/10.1002/gj.3993.

Schilling, J.G., Thompson, G., Kingsley, R., Humphris, S., 1985. Hotspot-migrating ridge interaction in the South Atlantic. Nature 313 (5999), 187–191. https://doi.org/10.1038/313187a0.

Seber, D., Barazangi, M., Ibenbrahim, A., Demnati, A., 1996. Geophysical evidence for lithospheric delamination beneath the Alboran sea and Rif-Betic mountains. Nature 379, 785–790. https://doi.org/10.1038/379785a0.

Segev, A., 2002. Flood basalts, continental breakup and the dispersal of Gondwana: evidence for periodic migration of upwelling mantle flows (plumes). Stephan Mueller Spec. Publ. Ser. 2, 171–191. https://doi.org/10.5194/smsps-2-171-2002.

Seton, M., Müller, R.D., Zahirovic, S., Gaina, C., Torsvik, T., Shephard, G., Talsma, A., Gurnis, M., Turner, M., Maus, S., Chandler, M., 2012. Global continental and ocean basin reconstructions since 200 Ma. Earth-Sci. Rev. 113 (3–4), 212–270. https://doi.org/10.1016/j.earscirev.2012.03.002.

Sial, A.N., 1976. The post-Paleozoic volcanism of northeast Brazil and its tectonic significance. An. Acad. Bras. Cienc. 48, 299–311.

Smith, P.E., Evensen, N.M., York, D., Szatmari, P., Oliveira, D.C., 2001. Single-crystal ^{40}Ar-^{39}Ar Dating of Pyrite: No Fool's Clock. Geology 403–406. https://doi.org/10.1130/0091-7613(2001)029<0403:SCAADO>2.0.CO;2.

Souza, S.Z., Vasconcelos, P.M., Nascimento, M.A.L., Silveira, F.V., Paiva, H.S., Dias, L.G. S., Thiede, D., Carmo, I.O., 2003. ^{40}Ar/^{39}Ar geochronology of Mesozoic and Cenozoic magmatism in NE Brazil. Short Pap. - IV South Am. Symp. Isot. Geol. 691–694.

Stewart, K., Turner, S., Kelley, S., Hawkesworth, C., Kirstein, L., Mantovani, M., 1996. 3-D, ^{40}Ar-^{39}Ar geochronology in the Paraná continental flood basalt province. Earth Planet. Sci. Lett. 143, 95–109. https://doi.org/10.1016/0012-821x(96)00132-x.

Stica, J.M., Zalán, P.V., Ferrari, A.L., 2014. The evolution of rifting on the volcanic margin of the Pelotas Basin and the contextualization of the Paraná-Etendeka LIP in the separation of Gondwana in the South Atlantic. Mar. Pet. Geol. 50, 1–21. https://doi.org/10.1016/j.marpetgTristan-Gough hotspoteo.2013.10.015.

Stone, P., Richards, P.C., Kimbell, G.S., Esser, R.P., Reeves, D., 2008. Cretaceous dykes discovered in the Falkland Islands: implications for regional tectonics in the South Atlantic. J. Geol. Soc. 165 (1), 1–4. https://doi.org/10.1144/0016-76492007-072.

Stone, P., 2013. Mesozoic dyke swarms of the Falkland Islands (South Atlantic). Geology and Regional Geophysics Programme, Internal Report OR/13/026, Keyworth, Nottingham, British Geological Survey, 27p.

Stracke, A., Hofmann, A.W., Hart, S.R., 2005. FOZO, HIMU, and the rest of the mantle zoo. Geochem. Geophys. 6 (5), Q05007. https://doi.org/10.1029/2004GC000824.

Stroncik, N.A., Trumbull, R.B., Krienitz, M.S., Niedermann, S., Romer, R.L., Harris, C., Day, J.M.D., 2017. Helium isotope evidence for a deep-seated mantle plume involved in South Atlantic breakup. Geology 45, 827–830. https://doi.org/10.1130/G39151.1.

Sun, S.S., McDonough, W.F., 1989. Chemical and isotopic systematics of oceanic basalts: implications for mantle composition and processes. Geol. Soc. Spec. Publ., London 42 (1), 313–345. https://doi.org/10.1144/GSL.SP.1989.042.01.19.

Svensen, H.H., Torsvik, T.H., Callegaro, S., Augland, L., Heimdal, T.H., Jerram, D.A., Planke, S., Pereira, E., 2018. Gondwana Large Igneous Provinces: plate reconstructions, volcanic basins and sill volumes. In: Sensarma, S., Storey, B.C. (Eds), Large Igneous Provinces from Gondwana and Adjacent Regions. Geol. Soc. London Spec. Pub. 463, 17-40. https://doi.org/10.1144/SP463.7.

Thiede, D.S., Vasconcelos, P.M., 2010. Paraná flood basalts: Rapid extrusion hypothesis confirmed by new ^{40}Ar/^{39}Ar results. Geology 38, 747–750. https://doi.org/10.1130/G30919.1.

Thompson, R.N., Gibson, S.A., Dickin, A.P., Smith, P.M., 2001. Early Cretaceous basalt and picrite dykes of the Southern Etendeka Region, NW Namibia: Windows into the role of the Tristan mantle plume in Paraná-Etendeka magmatism. J. Petrol. 42, 2049–2208. https://doi.org/10.1093/petrology/42.11.2049.

Thompson, R.N., Riches, A.J.V., Antoshechkina, P.M., Pearson, D.G., Nowell, G.M., Ottley, C.J., Dickin, A.P., Hards, V.L., Nguno, A.-K., Niku-Paavola, V., 2007. Origin of CFB magmatism: Multi-tiered intracrustal picrite-rhyolite magmatic plumbing at Spitzkoppe, Western Namibia, during Early Cretaceous Etendeka magmatism. J. Petrol. 48, 1119–1154. https://doi.org/10.1093/petrology/egm012.

Torsvik, T.H., Smethurst, M.A., Burke, K., Steinberger, B., 2006. Large igneous provinces generated from the margins of the large low-velocity provinces in the deep mantle. Geophys J. Int. 167 (3), 1447–1460. https://doi.org/10.1111/j.1365-246X.2006.03158.x.

Trumbull, R.B., Vietor, T., Hahne, K., Wackerle, R., Ledru, P., 2004. Aeromagnetic mapping and reconnaissance geochemistry of the Early Cretaceous Henties Bay-Outjo dike swarm, Etendeka Igneous Province, Namibia. J. Afr. Earth Sci. 40 (1–2), 17–29. https://doi.org/10.1016/j.jafrearsci.2004.07.006.

Trumbull, R.B., Reid, D.L., de Beer, C., van Acken, D., Romer, R.L., 2007. Magmatism and continental breakup at the west margin of southern Africa: A geochemical comparison of dolerite dikes from northwestern Namibia and the Western Cape. S. Afr. J. Geol. 110 (2–3), 477–502. https://doi.org/10.2113/gssajg.110.2-3.477.

Turner, S., Regelous, M., Kelley, S., Hawkesworth, C., Mantovani, M., 1994. Magmatism and continental break-up in the South Atlantic: high precision ^{40}Ar/^{39}Ar geochronology. Earth Planet. Sci. Lett. 121, 333–348. https://doi.org/10.1016/0012-821X(94)90076-0.

Ultsch, A., Vetter, C., 1994. Self-Organizing-Feature-Maps versus Statistical Clustering Methods: A Benchmark. Univ. Marburg, FG 1–14.

Ures, C., Bossi, J., Feraud, G., Bertrand, H., 1997. New age and geochemical constraints on the Paraná flood volcanism: additional data on Uruguay extrusive and intrusive formations. AGU 1997 Fall Meeting Abstracts.

Valente, S., Dutra, T., Heilbron, M., Szatmari, P., 2009. Litogeoquímica de diques de diabásio da Faixa Colatina, ES. Geochim. Bras. 23 (2), 177–192.

VanDecar, J.C., James, D.E., Assumpção, M., 1995. Seismic evidence for a fossil mantle plume beneath south America and implications for plate driving forces. Nature 378, 25–31. https://doi.org/10.1038/378025a0.

Velázquez, V.F., Riccomini, C., Gomes, C.B., Kirk, J., 2011. The Cretaceous alkaline dyke swarm in the central segment of Asunción rift, Eastern Paraguay: its regional distribution, mechanism of emplacement, and tectonic significance. J. Geol. Res. 2011,. https://doi.org/10.1155/2011/946701 946701.

Vesanto, J., Alhoniemi, E., 2000. Clustering of the self-organizing map. IEEE Trans. Neural Networks 11, 586–600. https://doi.org/10.1109/72.846731.

White, R., McKenzie, D., 1989. Magmatism at rift zones: the generation of volcanic continental margins and flood basalts. J. Geophys. Res. 94 (B6), 7685–7729. https://doi.org/10.1029/JB094iB06p07685.

Wigand, M., Schmitt, A.K., Trumbull, R.B., Villa, I.M., Emmermann, R., 2004. Short-lived magmatic activity in an anorogenic subvolcanic complex: ^{40}Ar/^{39}Ar and ion microprobe U-Pb zircon dating of the Erongo, Damaraland, Namibia. J. Volcanol. Geotherm. Res. 130, 285–305. https://doi.org/10.1016/S0377-0273(03)00310-X.

Will, T.M., Frimmel, H.E., Pfänder, J.A., 2016. Möwe Bay Dykes, Northwestern Namibia: Geochemical and geochronological evidence for different mantle source regions during the Cretaceous opening of the South Atlantic. Chem. Geol. 444, 141–157. https://doi.org/10.1016/j.chemgeo.2016.08.040.

Wilson, J.T., 1973. Plumes and plate motions. Tectonophysics 19 (2), 149–164.

Wilson, M., Guiraud, R., 1992. Magmatism and rifting in Western and Central Africa, from Late Jurassic to Recent times. Tectonophysics 213, 203–225. https://doi.org/10.1016/0040-1951(92)90259-9.

Zhou, H., Hoernle, K., Geldmacher, J., Hauff, F., Homrighausen, S., Garbe-Schönberg, D., Jung, S., 2020. Geochemistry of Etendeka magmatism: Spatial heterogeneity in the Tristan-Gough plume head. Earth Planet. Sci. Lett. 535,. https://doi.org/10.1016/j.epsl.2020.116123 116123.